Design and Analysis of Multi-DoF MEMS Gyroscope for Inertial Navigation using SOI-MUMPs Fabrication Process

Author

Adnan Shujah

00000205605

Supervisor

Dr. Muhammad Mubasher Saleem

DEPARTMENT OF MECHATRONICS ENGINEERING

COLLEGE OF ELECTRICAL & MECHANICAL ENGINEERING

NATIONAL UNIVERSITY OF SCIENCES AND TECHNOLOGY

ISLAMABAD

December, 2020

Design and Analysis of Multi-DoF MEMS Gyroscope for Inertial Navigation using SOI-MUMPs Fabrication Process

Author

ADNAN SHUJAH

00000205605

A thesis submitted in partial fulfillment of the requirements for the degree of

MS Mechatronics Engineering

Thesis Supervisor:

DR. MUHAMMAD MUBASHER SALEEM

Thesis Supervisor's Signature:

_____

DEPARTMENT OF MECHATRONICS ENGINEERING

COLLEGE OF ELECTRICAL & MECHANICAL ENGINEERING

NATIONAL UNIVERSITY OF SCIENCES AND TECHNOLOGY,

ISLAMABAD

December, 2020

Declaration

I certify that this research work titled "*Design and Analysis of Multi-DoF MEMS Gyroscope for Inertial Navigation using SOI-MUMPs Fabrication Process"* is my own work. The work has not been presented elsewhere for assessment. I have properly acknowledged / referred the material that has been used from other sources.

Signature of Student

Adnan Shujah

00000205605

Language Correctness Certificate

This thesis has been read by an English expert and is free of typing, syntax, semantic, grammatical and spelling mistakes. Thesis is also according to the format given by the university.

Signature of Student

Adnan Shujah

00000205605

Signature of Supervisor

Copyright Statement

- Copyright in text of this thesis rests with the student author. Copies (by any process) either in full, or of extracts, may be made only in accordance with instructions given by the author and lodged in the Library of NUST College of E & ME. Details may be obtained by the Librarian. This page must form part of any such copies made. Further copies (by any process) may not be made without the permission (in writing) of the author.
- The ownership of any intellectual property rights which may be described in this thesis is vested in NUST College of E & ME, subject to any prior agreement to the contrary, and may not be made available for use by third parties without the written permission of the College of E & ME, which will prescribe the terms and conditions of any such agreement.
- Further information on the conditions under which disclosures and exploitation may take place is available from the Library of NUST College of E & ME, Rawalpindi.

Acknowledgements

Above all else, acclaims and gratitude to Allah Almighty for his showers of blessings for the duration of the life and to finish this examination work effectively

I might want to communicate my profound and earnest gratitude to my research supervisor Dr. Muhammad Mubasher Saleem (Associate HOD, Department of Mechatronics Engineering, College of E&ME, NUST) for giving me the chance to do the exploration and giving priceless direction all through the research. His elements, vision, genuineness and inspiration profoundly motivated me. He has shown me the procedure how to do the exploration and furthermore the technique how to introduce the work as unmistakably as could be expected under the circumstances. I am grateful for what he had offered me. Besides, I am also thankful for his friendship and empathy. I might likewise want to thank Dr. Umar Shahbaz Khan and Dr. Amir Hamza for guiding me through thesis and evaluation committee.

I am extremely grateful to my parents for their continuous support, love, care and sacrifices to make me prepared for the future through education. I am very much thankful to my wife, Fadaiqa and my daughters, Unza Adnan and Amal Adnan for their love, prayers and continuous support to complete this research.

Special thanks go to my friends Syed Ali Raza, Shayaan Saghir, Ahmad Raza, Zawar-ul-Hassan, Afnan Yaqoob and Azka Asif for the keen interest shown to complete this research.

I am also very much thankful to the Department of Mechatronics Engineering and my University, NUST to consider my services and offer me this MS under the career development program.

I dedicate this work to my adored parents for nursing me throughout the life with affections and love and my beloved siblings who always inspired me to do this great accomplishment

Abstract

The dissertation presents the design of an electrostatically actuated multi-DoF micro-electro-mechanical system (MEMS) gyroscope having the 1-DOF in the sensing mode while 2-DOF in driving mode. MEMS gyroscope are used in multiple applications such as inertial navigation, in automobiles, image stabilization and many other potential applications. The main emphasis in this effort is to propose a non-resonant gyroscope, having multi-degree-of-freedom(multi-DoF) and it follows the design limitations of SOI-MUMPs fabrication process which is commercially available and is offered by MEMSCAP Inc, USA. The optimization is based on the device dimensions and layout using the parametric optimization technique. The proposed device is having the bandwidth of 1772 Hz with an average dynamic amplification of 2.89 within the flat operation region and having the sensitivity of $3.27\ mV/°/s$. The finite element analysis (FEM analysis) of the device is simulated in ANSYS.

Key Words: *MEMS, Gyroscope, Non-Resonant, multi-DoF, Electrostatic, FEM.*

Table of Contents

List of Figures

List of Tables

Acronyms

MEMS	Micro-electro-mechanical Systems
FEM	Finite Element Method
DoF	Degree of Freedom
DVA	Dynamic Vibration Absorber

Chapter 1: Introduction

The research work focuses on the design and analysis of MEMS vibratory, non-resonant, multi-DoF gyroscope for inertial navigation. First, a motivation and scope of this work is briefly discussed. Second, an introduction of MEMS gyroscopes is discussed. Third, discussion on the fabrication processes is presented and finally the actuation and sensing mechanisms for MEMS devices are discussed in this chapter.

1.1 Motivation and Scope

Throughout the world, the word "miniaturization" is one of the key factors that is boosting the motivation of the research and development of the different devices. Also, the rising demand of low power, more efficient, light weight, small in size and more reliable devices are the demand of current technology advancements.

The famous speech of the, Richard Feynman on December 26, 1959 titled, "*there is plenty of room at the bottom*", described the importance and benefits of miniaturization of devices and their uses [1]. With times, the invention of the transistors has opened the door for miniaturization. Integrated circuit (IC) technology enables us to place a transistor to a place that is few thousands of an atom. In today's world, the use of the MEMS (micro-electro-mechanical systems) is realized in different fields. Among these devices, the inertial sensors achieved a reasonable space due to their high performance, reliability and miniaturization. The properties of inertial sensors of low power consumption and small size make their acceptance in the field and increase the areas of applications. Presently, they have been used in navigation of air vehicles, marine vehicles and in various stabilization systems.

For most of the MEMS devices fabrication, inhouse fabrication processes are available. These fabrication processes are good enough for the fabrication of a few devices but not capable of the mass production. A commercial and a reliable micro-fabrication process of SOIMUMPs is available with defined design rules.

With the increasing demand of MEMS inertial sensors and availability of the commercial fabrication processes, there is enough motivation to investigate more optimal and miniature MEMS devices.

1.2 Definition of MEMS

MEMS, stands for "*Micro-Electro-Mechanical Systems*" and mostly known as the micromachines or microsystem, is a technology which combines the micro level electrical systems and mechanical systems. Practically a device having the dimensions of micro-meters (1µm $=10^{-6}\,m$) and fabricated using any of the available MEMS level fabrication method, utilizes both electrical and mechanical functions [2]. The MEMS devices are generally range in sizes of few micrometres to millimetres. The central unit of MEMS device, process the data and they interact with outside structures of micro-actuators and micro-sensors. The millimetre sized MEMS devices are generally termed like *"meso-scale MEMS devices"*. Figure1.1 shows the dimensions of the MEMS devices in comparison with other devices.

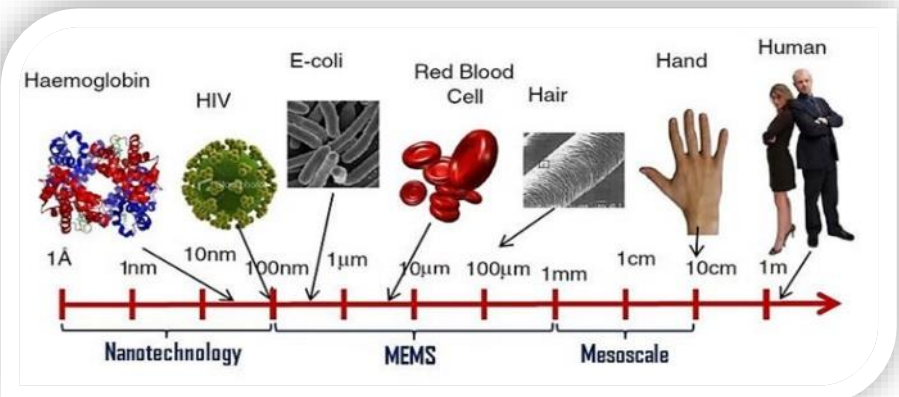

Figure 1.1 Comparison of MEMS devices with Nano and Meso scale devices. (Adapted from Nguyen et al. [3])

Technology of the MEMS is evolved from the integration (IC) technology. MEMS actuators, sensors and other structures are co-fabricated in silicon. Since then, the industries and governments strongly promote the MEMS technology and there is a remarkable progress in this field. With the progress and evolution many manufacturing techniques have been evolved. A number of MEMS devices have been fabricated using the silicon and different fabrication processes like surface micromachining, bulk micromachining, lithography, molding (LIGA) Process and SOIMUMPs. The batch fabrication, low cost, small size, reliability, robustness are the key features of the MEMS devices which makes them a product of choice in many fields of industries.

1.3 MEMS Applications

A complete system on a single chip, revolutionize almost every product category. With the advancements in MEMS technology, it brings together and also expands the horizon of design and applications of smart devices.

Table 1: MEMS devices applications in different fields. Redrawn from reference [4]

Automobile	**Electronics devices**	**Medical field**	**Communication Equipment**	**Defence Equipment**
Sensor for Internal - Navigation	Heads for Disk Drives	Blood-pressure Measuring Sensors	Components of network for fibre-optics	Mutation guidance-systems
Sensors for Air Conditioning (Compressor)	Heads of Ink jet Printers	Muscles Simulator & Systems for Drug Delivery	Switches and RF Relays	Surveillance-systems
Sensors for Brakes -force Calculation	Projection Screens-Television	Implanted Sensors to Monitor Pressure	Instrumentation and Portable Devices Projection-displays	Arming-Equipment and systems
Fuel Sensors for Level Detection	Sensors for Earthquake	Prosthetic Limb Sensors	Voltage control oscillators	Embedded-System Sensors
Sensors with Airbag	Sensors used in Avionics (pressure sensors)	Small Analytical Medical Instruments	Couplers and Splitters	Storage of Data
“Intelligent” Tires	Storage Systems of Mass-data	Heart Pacemakers	Lasers (Tuneable)	Controls for Aircrafts

1.4 Introduction to MEMS Vibratory Gyroscope

The word "*gyroscope*", is derived from the old Greek language, generally it is referred to mechanical gyroscopes. The gyroscope is used for measuring orientation and it works on the momentum conservation principle.

1.4.1 The Coriolis Effect

MEMS vibratory gyroscope works on "*Coriolis effect*", by using this principle the transfer of the energy between the quadrature modes of drive and sense modes take place [5] The drive mode mass oscillates at a constant amplitude and due to the input angular velocity, the sense mode measured orthogonal oscillations [6,7]. For the sensing of the angular velocity MEMS gyroscopes use mechanical structures those are vibrating. Miniaturization in the mems devices is possible because they have don't have the rotating elements those require bearings to rotate. Figure 1.2 shows the motion of ball in straight line over a frictionless surface rotating with an angular velocity of ω. The ball is moving in a straight line with a constant linear velocity, with respect to stationary observer and there is no effect of rotation of the surface. But on the other hand, the observer fixed to the surface perceives totally different motion of the ball. He perceives as an unknow force is accelerating the ball in opposite direction of the rotation while the ball is approaching the edge of the surface. The dotted curved line shown in the figure 1.2 is the perceived path by moving observer, while the ball is moving in a straight line with respect to an observer who is stationary. This whole phenomenon is known as "*Coriolis effect*" and the acceleration is known as the "*Coriolis acceleration"* as presumed by the rotating person. [8]

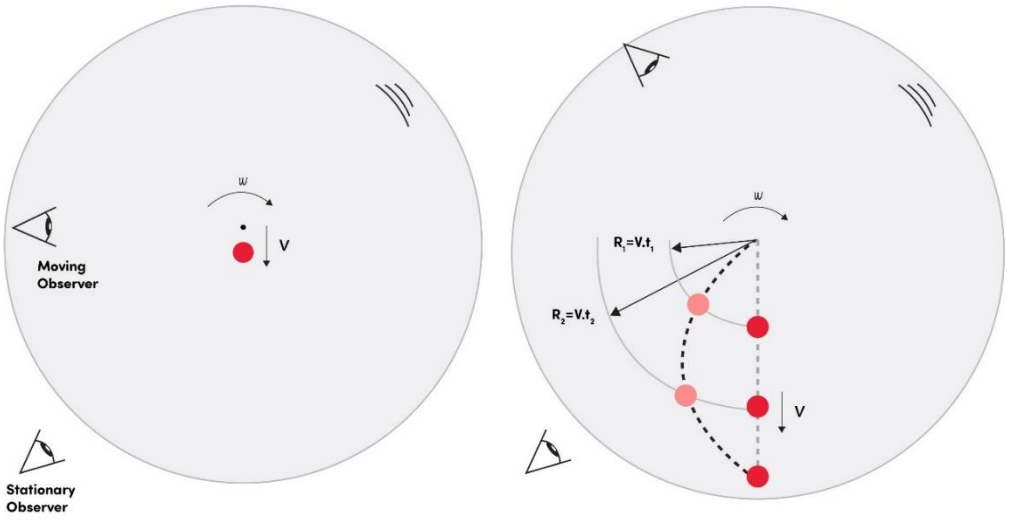

Figure 1.2 The Coriolis effect shown by the ball slides over the rotating disc surface. Redrawn from reference [8]

The magnitude of the Coriolis force and its direction are calculated as

$$a_c = -2\,\Omega \times V \tag{1.1}$$

Where "V" represents the object velocity and the "Ω" represents the velocity-vector for angular velocity having the magnitude which is equal to rate of the rotation "ω" and its direction is parallel to the axis of the rotation of the reference frame which is rotating, and cross-product operator is represented by the " × " symbol.

The formula shown in equation 1.1 shows that acceleration produced will be perpendicular to the frame of the rotational axis and the mass-velocity that is moving and known as "*Coriolis acceleration''*.

To express the relation of the Coriolis force, multiply the equation (1.1) with the mass of the relevant object.

$$F_c = -2m\Omega \times V \tag{1.2}$$

.

1.4.2 MEMS Vibratory Gyroscope

Figure 1.3. shows a mass which is suspended by two sets of springs those are perpendicular to each other (x-axis and y-axis) and this forms a typical model for vibratory gyroscope.

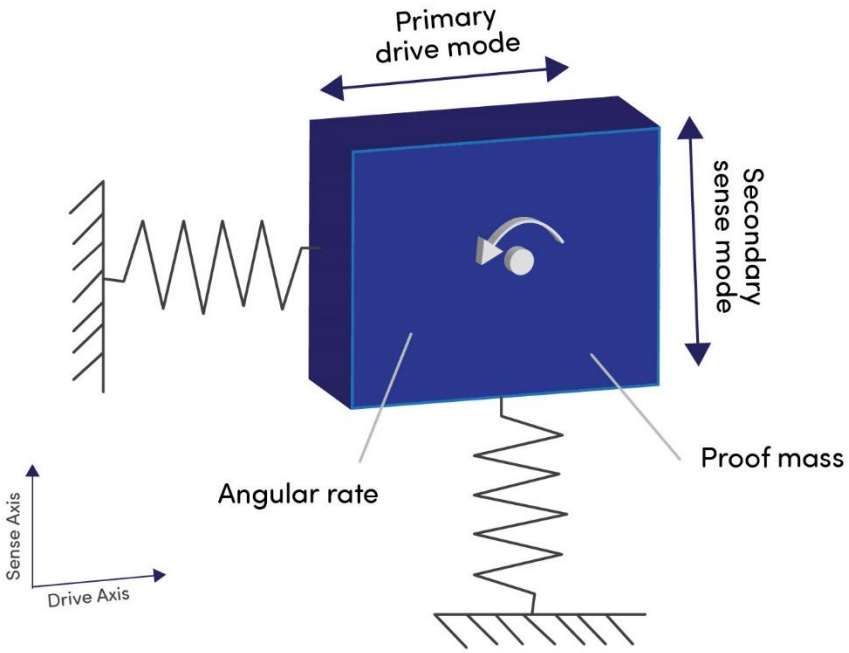

Figure 1.3 MEMS vibratory gyroscope working principle.

The system mentioned in figure 1.3 is the model for MEMS vibratory gyroscope having the two vibration modes those are at right-angle to each other. Driving-mode vibrations corresponds to the x-axis and the sensing-mode vibrations corresponds to the y-axis. ω_x and ω_y are the vibration frequencies of drive and sense modes respectively. A driving force, $F_d(t)$,which is an electrostatic force is applied in x-axis on the mass known as driving mass. If a driving force,F_0 is applied constantly and the frequency of this driving force is w_d,then the corresponding electrostatic sinusoidal driving force will be

$$F_d(t) = F_0 cos\, w_d(t) \tag{1.3}$$

If there comes a rotation about a certain axis which is the z-axis in this case and is out of the paper plane, having the angular velocity of Ω, an alternating force is generated and acted in the y-direction due to the Coriolis effect. In the result, the system vibrates with the frequency of ω_y in the y-

direction. Thus, a mass m with velocity of $v(t)$ moving in the x-direction will experience a Coriolis force $F_C(t)$ along y-direction.

$$F_C(t) = -2mv(t) \times \Omega \qquad 1.4$$

To determine the angular velocity, some sensing techniques need to be implemented to measure the vibrational amplitude in the y-direction (sense direction) [9]

1.4.3 Classification of MEMS Vibratory Gyroscope

The micromachined vibratory gyroscopes (MVGs) have been divided into two sub-categories, (a) angle-gyroscopes and (b) rate-gyroscopes. The one known as angle-gyroscopes measure the orientation angle and the other one known as rate-gyroscopes measure the rotational rate.

The highest performance gyroscopes are the angle gyroscopes. They have been divided in to subcategories depending on their shape and designs. From the subcategories of the angle gyroscopes vibrating ring and the hemispherical resonating gyroscopes are the only realizable candidates for the inertial navigation due to fabrication limitations. On other hand the rate gyroscopes are categorized in "resonant" and "non-resonant" gyroscopes depending on their working principles [10].

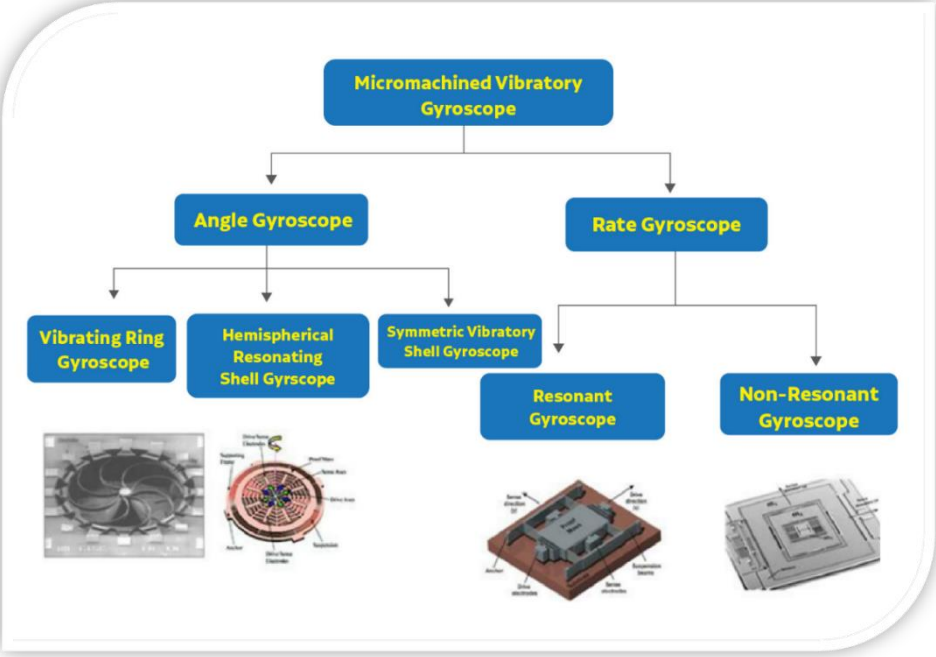

Figure 1.4 Classification of the micromachined vibratory gyroscopes [10]

1.4.4 Resonant and Non-Resonant Gyroscope

The “resonant gyroscopes”, have been operated at the resonance to obtain the high mechanical gain and sensitivity [5,11-16]. In resonant gyroscopes the drive and sense masses need to operate at same resonance frequencies. The low gain outside the small area of resonance and the narrow bandwidth are the major concerns of the resonant gyroscopes. While in the case of non-resonant gyroscopes, the gyroscopes are designed and also tuned to operate in between the flat/nearly-even region between the resonant-frequencies to achieve the maximum robustness in case of the parametric variations due to fabrication process limitations and the environmental fluctuations.

1.4.5 Advantages of the Non-Resonant Gyroscopes

In resonant gyroscopes the drive and sense masses need to operate at same resonance frequencies. The low gain outside the small area of resonance and the narrow bandwidth are the major concerns of the resonant gyroscopes. To cater these issues the techniques of the active tuning [17] and feedback control system [18] have been deployed. Various techniques have been available in literature to cater these issues of the resonant gyroscopes, one of the feasible solutions is the multi-degree of freedom gyroscopes also known as non-resonant gyroscopes.

The main advantage of non-resonant gyroscopes over the resonant gyroscopes is in terms of robustness characteristics. The parametric variations due to fabrication process limitations and the environmental fluctuations have the least effect on non-resonant gyroscopes. To relax or avoid the advanced control techniques, wider bandwidth is achieved in case of non-resonant gyroscopes.

Figure 1.5, provides a summary to choose the various design choices to fabricate the vibrating MEMS gyroscope with over twenty-five hundred (2500) potential combinations.

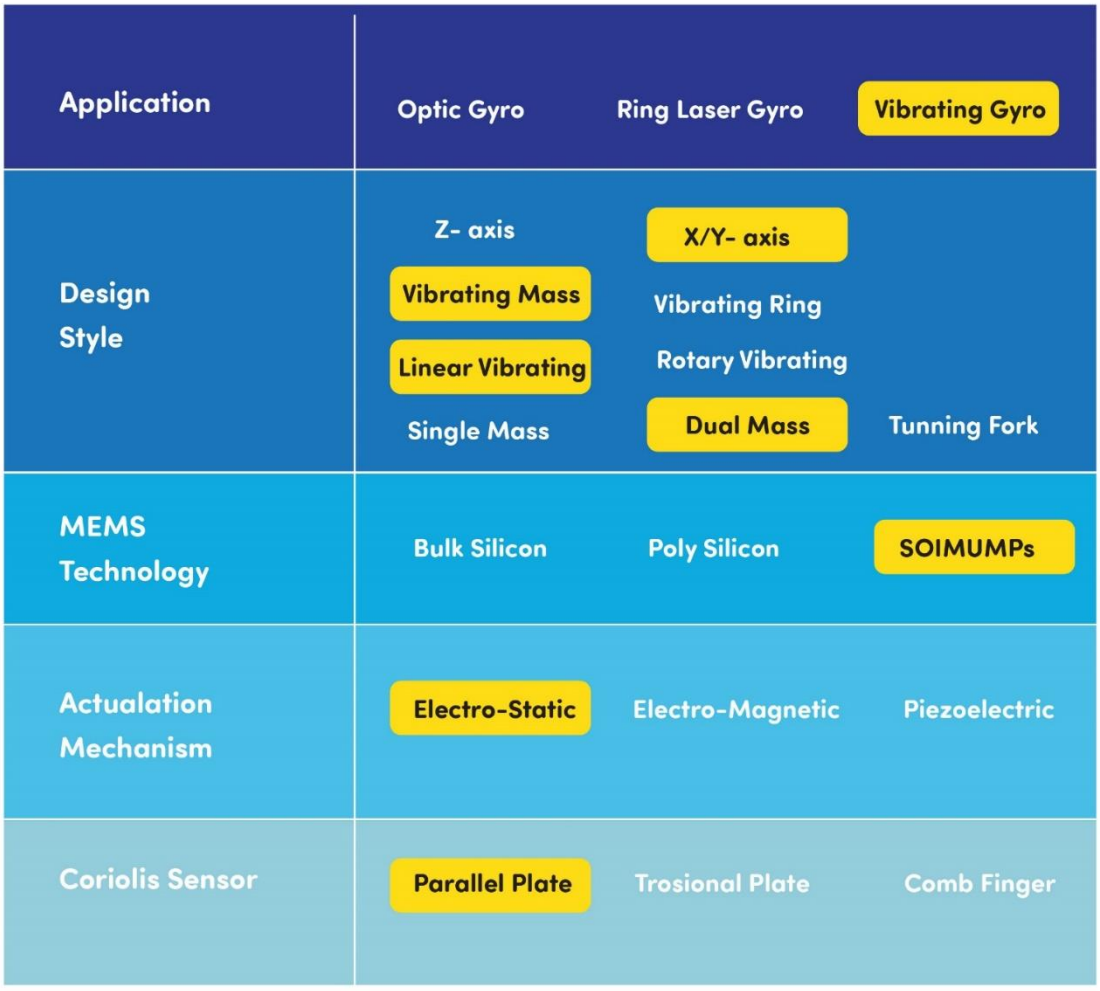

Figure 1.5 Various potential combinations for designing the micromachined vibratory gyroscopes.

1.5 Microfabrication Process

To fabricate the MEMS devices, different fabrication processes are available. These fabrication processes differ from each other on the basis of material used in fabrication of MEMS devices, type of the device, feature size and the cost involved**.** MUMPs stands for multi-user MEMS process.

1.5.1 LIGA

The acronym LIGA, stands for Lithographie (lithography), Galvanoformung (electroplating) and Abformung (molding). LIGA is one of the MEMS fabrication technique, usually used to produce high aspect ratio designs and structures. Two main types of LIGA fabrication technologies are available, X-ray based and UV based LIGA techniques. For high aspect ratio, X-ray based fabrication is used while for low aspect ratio, UV based fabrication is used for designs and which is more commonly used. This process consists of three main steps: (a) Lithography, (b) electroplating and (c) molding [19].

1.5.2 Metal-MUMPs

The process of Metal-Mumps fabrication uses a metal electroplating to fabricate MEMS devices. Nickel, a metal is used for whole device fabrication in this process. Few MEMS devices like microgrippers have been fabricated using this process [20]. However, Metal-Mumps is not suitable for fabricating the devices with biomedical applications, as of high coefficient of thermal conductivity. High temperatures could damage the object under manipulation.

1.5.3 Poly-MUMPs

Poly-MUMPs stands for polysilicon multi-user MEMS process. MEMS sensors are fabricated using the process of Poly-MUMPS. It has three layers, one of the layers is the metal layer and the other two layers are sacrificial layers. In this process about seven layers can be formed using up to eight masks. 2 μm is the minimum feature size for this process. Silicon have very different properties from polysilicon [21].

1.5.4 SOIMUMPs

A standard and commercially available, low cost process for the fabrication of microstructures is available and is known as the *Silicon-on-Insulator Multi-User-MEMS* micro level fabrication process (SOIMUMPs) offered by a very well-known and a reliable foundry MEMSCAP Inc. located in United States of America (USA). In this process the substrate under the moveable structures get removed during the etching process and thus this process allows the least air damping. The attribute of fabricating the high aspect ratio micro-structures make its very suitable for the fabrication of the high-performance MEMS devices. The cross-section view of the SOIMUMS process is shown in the figure 1.6 [22]

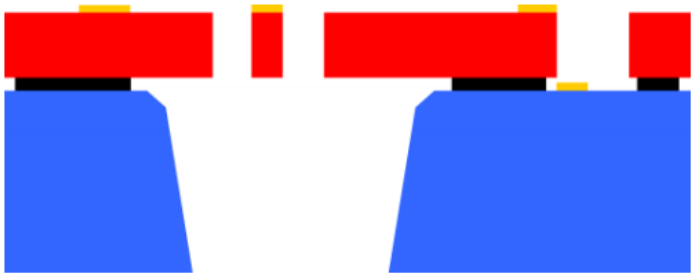

Figure 1.6 MEMSCAP SOIMUMPs fabrication process cross-section view showing all the layers [22]

The process has 04 masks for patterning on silicon on insulator (SOI) wafer and its etching. In the figure 1.6, the doped polysilicon structural layer is shown in red color and this layer is anchored to the substrate with the help of oxide layer. Adjacent metal pads are electrically isolated by introducing the grooves in the structural layer. As per the designed rules of this process as mentioned in the SOIMUMPs design handbook [22], the thickness of the silicon layer could be 25±1 μm with the thickness 2±0.1 μm for oxide layer and 400±5 μm of handle wafer (substrate). The minimum feature width of the structure must be 6 μm for the structure length of 200 μm and above. The design limitations of the SOIMUMPs fabrication process puts certain constraints on the designers. Following design constraints/limitations have been considered during the proposed design of the micromachined gyroscope.

Limitation-1: No electrical lines run across the trenches in the device due to the non-arability of top and bottom cap after etching. Electrode pads could not be the part of the design as they cannot be attached to the inner electrodes. Due to these constraints' designers have only choice of the in-plane sensing and actuation techniques.

Limitation-2: Due to the etching process the bottom cap is missing and hence do not allow the central anchor to be designed in the device as shown in the figure 1.7. Therefore, the proposed design of the gyroscope in comparison to the traditionally available gyroscopes in literature differs and we cannot enclose the inner most mass within another mass which is against the design rules of SOIMUMPs Fabrication guidelines.

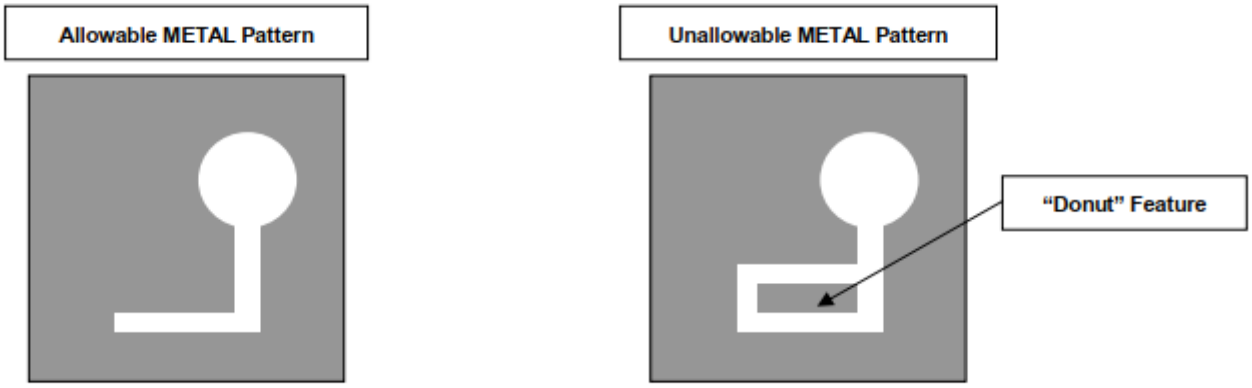

Figure 1.7 Allowable and unallowable feature for metal masking in the SOIMUMPs fabrication process [22]

Limitation-3: Figure 1.6 shows the structural layer in red color made of silicon where the device is patterned. Less than the 33% of the chip area should be etched, which limits the designer to have a certain amount of the gap with in the structures and the number of folds of the springs. The designer has to reduce the unused area and also need to reduce the air gaps between the masses.

Table 2: Material properties extracted from the CoventorWare material library for SOIMUMPs TM fabrication process.

Material Properties (Units)/Materials	**Silicon**
$Young's\ Modulus\ GPa$	169
$Poison\ Ratio$	0.29
$Density\ (Kg/m^3)$	2500

1.6 Actuation and Sensing Mechanisms in MEMS Devices

To drive the device an actuation mechanism is needed, similarly to calculate the output of the device a sensing mechanism have to be placed. Depending upon the working principles of sensors and actuators different types of mechanism are available in literature.

1.6.1 Actuation Mechanisms

Actuation mechanisms could be broadly classified in to five categories depending upon their working principles which include Electro-thermal, electrostatic, electromagnetic, piezoelectric and the shape memory alloy actuators.

In the Electro-thermal actuators [23,24] the force generated is dependent on the thermal expansion of the materials. Under the very small excitation voltages they have capability to generate larger displacements. Due to the limitations of the working temperature range, temperature sensitive objects could not use these types of actuators. The electrostatic actuators [25,26] have the low power consumption, high frequency response and having no hysteresis. however, they need the high voltages to operate. There are two different configurations of the electrostatic actuators, the one is transverse and the second one is lateral comb drives. Electromagnetic actuators have the fast and quick response, having high response and their control is easy. They offer large displacements but their large physical size is the major issue. The piezoelectric actuators offer large output force with very compact dimensions and having good operational bandwidth. But these actuators offer very small displacements which limits its use in extensive applications. Finally, the shape memory alloy actuators [27] have large deformations, high working density and high recovery force. But they have very slow speed and hence low efficiency. Table 3 represents the summary of the actuators used in MEMS applications.

Table 3: Actuation mechanisms and their Comparison [28]

Actuator type	**Working principle**	**Pros**	**Cons**	**Example**
Electro-thermal	Thermal expansion	Large displacement low voltage dimension	High working temperature	[29,30]
Electrostatic	Electrostatic force	Frequency response is fast Power consumption is low No hysterics	Dimensions are large Problems of Pull-in Circuits are complicated	[31,32]
Shape-memory-Alloy	Materials deformation	Flexible low efficiency Frequency response is large	Hysterics Power consumption is large	[33,34]
Piezoelectric	Piezoelectric effect	Large force Good operational bandwidth	Displacement	[35-37]
Electromagnetic	Magnetization effect	Displacements are large linear effect Wearing negligible Response is quick Control is easy	Relatively large dimension Difficult to manufacture	[38]

1.6.2 Sensing Mechanisms

Capacitive sensors [39-41] are the sensors those can measure the force ranging from pN to mN scale. For high resolution detection they are mostly used with the electrostatic actuators. Capacitive

sensors work on the principle of change in capacitance and its measurements. This capacitance changes between the electrodes and the respective stator and this is done by moving the electrode shuttle. High sensitivity, larger bandwidth, large dynamic range and low power consumption are the key features of electrostatic sensors. But they need complex electronics. Electrothermal sensors follow the principle of the heat consumption from the device surface and the surrounding, differential measurement structures are employed for sensing calculations. They have high resolutions with small dimensions. These sensors have large power consumptions and having low response speed [42,43,44]

Piezo sensing works on the principle of piezoresistive effect and this technique have been widely used in MEMS. The mechanisms of transduction are used which could convert the mechanical distortions into the voltages. [45-46]. In MEMS Piezoelectric sensors are used widely as Resonators and transducers. Having the wide measurement range and wider bandwidth but heir manufacturing process are very complex.

Table 4 : Comparison of different sensing mechanisms used in MEMS. [28]

Sensor Type	**Working principle**	**Pros**	**Cons**	**Resolution**	**Examples**
Capacitive	Capacitive change	High sensitivity Large bandwidth Fast response speed	Large dimension Complicated circuit	μN	[47]
Electrothermal	Resistance change	Small dimension Simple structure High resolution	Low response speed Large consumption	μN	[42-44]
Piezoelectric	Piezoelectric effect	Measurement range is wide Extra voltage not needed Wider bandwidth	Complex manufacturing process Cannot work in high temperature	μN or sub-μN	[48,49]
Piezoresistive	Resistance change	Simple material High bandwidth Large frequency response	Sensitive to ambient temperature Hysterics Large power consumption	mN	[38]

Chapter 2: Literature Review

2.1 Designs from the Literature

In order to get the highest possible gain and increased sensitivity, usually in resonant rate gyroscopes, the frequencies of the drive mode and the sense mode are designed and/or tuned to match. But the fabrication imperfections and the operating condition fluctuations greatly affect the system response such that there exists a mismatch in the resonance frequencies of the drive-mode and the sense-mode which leads to reduced sensitivity and performance degradation [50,51-53].

Therefore, the resonant gyroscopes are designed in a way to operate at the resonant peak or very near to its resonant peak. To achieve the required degree of mode matching advanced control techniques and readout circuitry have been implemented [54-57].

The narrow bandwidth and low gain outside the vicinity of resonance are the prime concerns in case of resonant gyroscopes. At the cost of the reduced gain, systems with slighted shifted sense mass resonance frequency from the drive mass resonance frequency is available in literature [58].

To cater the above-mentioned issues in the resonant gyroscopes, different designs have been available in the literature which utilizes the concept of the multi-DoF systems to make MEMS vibratory non-resonant gyroscopes. These types of gyroscopes are called “non-resonant gyroscopes”, because they do not operate in mode matched condition but in the flat region between resonant frequencies where effect of parametric and environmental fluctuations is minimum.

A review of the previously done research work is carried out to design a multi-degree-of-freedom, non-resonant gyroscope considering the design constraints of the SOIMUMPs microfabrication process.

Table 5: MEMS "Non-Resonant Gyroscopes" available in the literature

	Structural Layer of device					
Reference	**Layer Material**	**Layer Thickness (um)**	**Device Configuration (DoF)**	**Size of the Device**	**Device Sensitivity**	**Device Bandwidth**
[59]	Polysilicon	2	Drive = 2 Sense = 2	$0.5 \times 0.7\ mm^2$	$0.72 \times 10^{-3} \mu m/°/s$	23 Hz
[60]	Polysilicon	100	Drive = 1 Sense = 2	-	$0.0308\ mV/°/s$	50 Hz
[58]	Silicon	75	Drive = 1 Sense = 2	-	$2.34\ \mu V/°/s$	600 Hz
[61]	Silicon	50	Drive = 1 Sense = 2	$3.0 \times 3.0\ mm^2$	$56\ \mu V/°/s$	250 Hz
[62]	Nickel	20	Drive = 2 Sense = 1	$2.6 \times 2.2\ mm^2$	$1.7\ \mu m/°/s$	2.11 kHz
[63]	Nickel	20	Drive = 2 Sense = 1	$1.6 \times 2.4\ mm^2$	$0.045\ fF/rad/s$, $0.052 \times 10^{-3} \mu m/°/s$	1.71 kHz
[64]	Nickel	20	Drive = 2 Sense = 1	$2.6 \times 2.2\ mm^2$	-	1.4 kHz
[65]	Nickel	9	Drive = 2 Sense = 1	$1.9 \times 2.0\ mm^2$	-	1.0 kHz
[66]	Nickel	20	Drive = 3 Sense = 1	$3.0 \times 3.2\ mm^2$	$0.565\ fF/rad/s$	3.0 kHz

The earliest design approach which utilized the concept of the dual-mass system in the drive-mode and was the very first attempt to utilized the concept of dynamic vibration absorber (DVA) was represented by Dyck et al. [67] shown in figure 2.1.

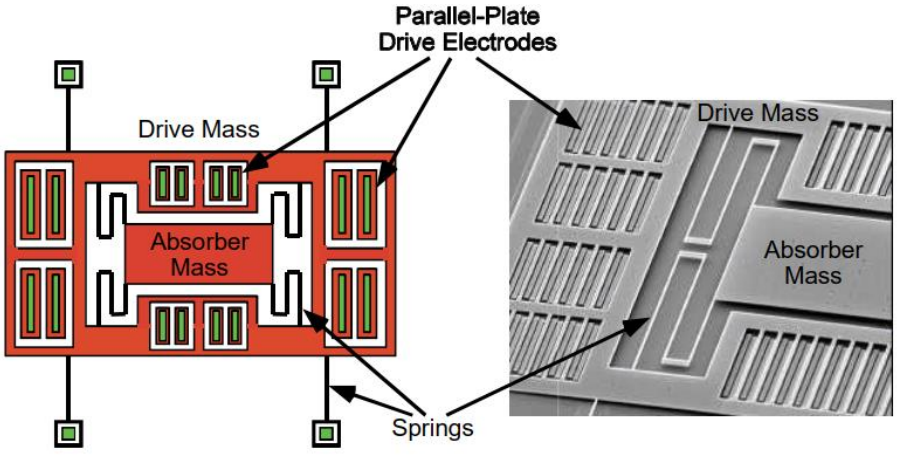

Figure 2.1 Prototype design of double-mass oscillator [67]

A 2-DoF system driven using the parallel plate actuation at antiresonance was demonstrated. An absorbing mass is connected to the driving mass with the help of the folded springs. The system shows that there is substantial motion amplification at antiresonance by the use of the dynamic vibration absorber (DVA) concept. The frequency response region near the antiresonance was approximately flat so it is difficult to exactly detect the value of the antiresonance frequency value. In the dual mass oscillator system, the second (absorber) mass may be insensitive to the partial variations in damping and strains.

Amplification and the bandwidth are controlled by monitoring the mass ratios "μ" and the frequency ratios "γ". The 1st and 2nd Resonant frequencies are dependent on the value of μ. As the value of μ decreases the frequency separation also decreases, which is one of the key points in designing the dual mass oscillator.

In the absence of the damping mechanism, the mechanical gain is infinite, whereas for operation in ambient conditions the damping mechanism, mainly viscous damping reduces the gain but it is still substantial. This is another way to see a dual mass oscillator as a "mechanical amplifier".

[59] proposed the gyroscope design having the 4-DOF and it uses the concept of the dynamic amplification to achieve the larger amplitude without matching the sense mass frequency with the drive mass frequency or simply without achieving the resonance, it also decouples the drive direction oscillations from sense oscillations by separating their motion using a decoupling frame design as clear from figure 2.2

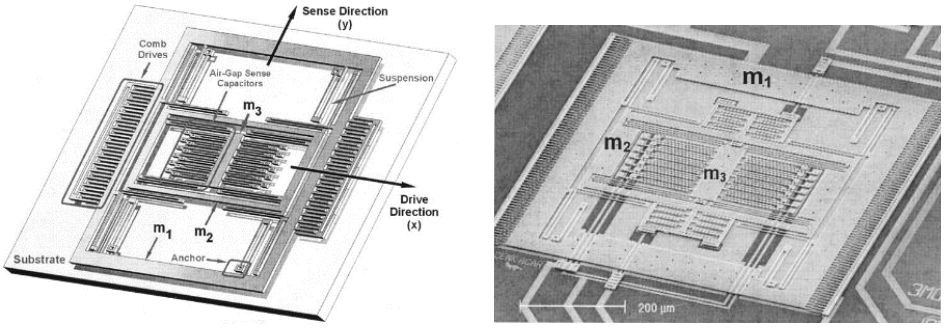

(a) (b)

·Figure 2.2 (a) Schematic diagram of the gyroscope having 4-DoF, having decoupled-modes for oscillations (b) fabricated prototype 4-DOF gyroscope.[59]

There are three proof masses in the design. The mass m_1 and the combined mass of $m_2$and m_3 form the drive oscillator, while the mass m_2 and m_3 form the sense direction oscillator. In both of the modes there is a nearly-even operation region between two resonant peaks. The operational region is the overlapped region of the antiresonance frequency band of the drive mass and the sense mass. The design used the concept of dynamic amplification in both drive mode as well as in the sense modes by using multiple masses. This, increased the bandwidth and reduces the sensitivity due to parameter fluctuations. This design improves the robustness and also relax the control system requirements.

[60] presented the non-resonant gyroscope design having the sense mode oscillator with two-DoF and Single-DoF in drive mode. There are two interconnected masses as m_1 and m_2. Masses $m_1$and m_2 are coupled to oscillate together in the direction of applied force to drive and form the Single -DoF drive mode while the mass which acts as absorber-mass is the m_2 in 2-DoF sense mode oscillator shown in figure 2.3.

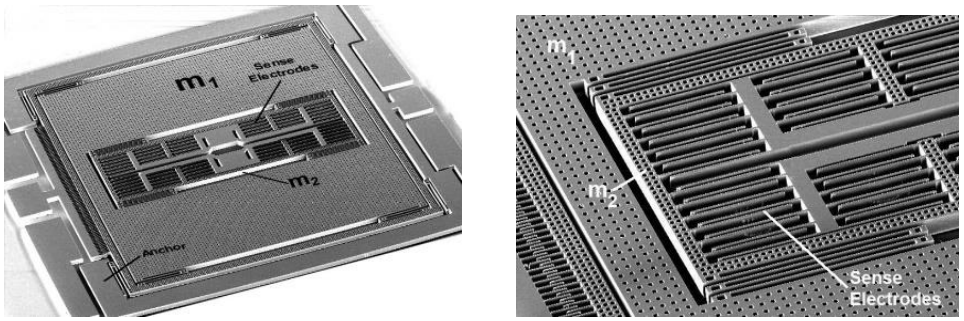

Figure 2.3 (a) Scanning electron micrograph of gyroscope with 1-DoF drive and 2-DoF sense mode. (b) Scanning electron micrograph of the differential sensing electrodes and the sense-mode passive. [60]

The two degree of the sense mass oscillator provides the two resonance peaks in sense direction instead of the single resonant peak which enhances the robustness of the system. The device is designed to work in the nearly even-region of the response-curve of the sense mode, as the response is safe to ambient changes and perturbations in this region. Mass m_2 is very small as compared to the mass m_1, this enables dynamic amplification, which improves the system response as a small Coriolis force acting on mass m_1 generates a much larger force on mass m_2.

In this design the mechanical systems are used to achieve the capability of disturbance -rejection and not by the compensation strategies and the active control system.

[58] represents the design of the MEMS based gyroscope having 1-DoF in the drive mode and 2-DoF in the sense mode. In this research work, authors analyzed the design tradeoffs which are associated with the incremental value of the operational frequency of the gyroscope by utilizing the concept of multi-DoF sense mode. They have designed three different variants with those having frequencies of their operation with 0.7kHz, 3.1kHz and 5.1 kHz with peak spacing of 150Hz, 400Hz and 600Hz respectively. Whereas the scale factors for the devices are found to be 14.2, 5.08 and 2.34 μV/°/s respectively. This shows that the scale factor reduces by increasing both the operational frequency and the bandwidth.

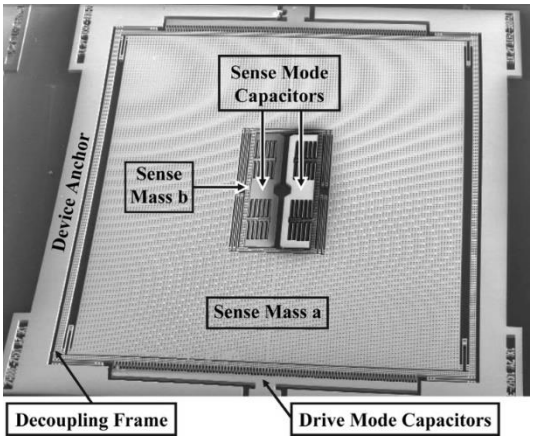

Figure 2.4 SEM image of the gyroscope after fabrication, having sense mode with 2-DoF [58]

[61] presented a gyroscope design for improved robustness, having the single degree-of-freedom (DoF) drive and the two degree-of-freedom (DoF) sense modes as shown in figure 2.5. The adjustment of the drive mode resonant frequency is done in such a way that it come between the two resonant peaks of sense mode.

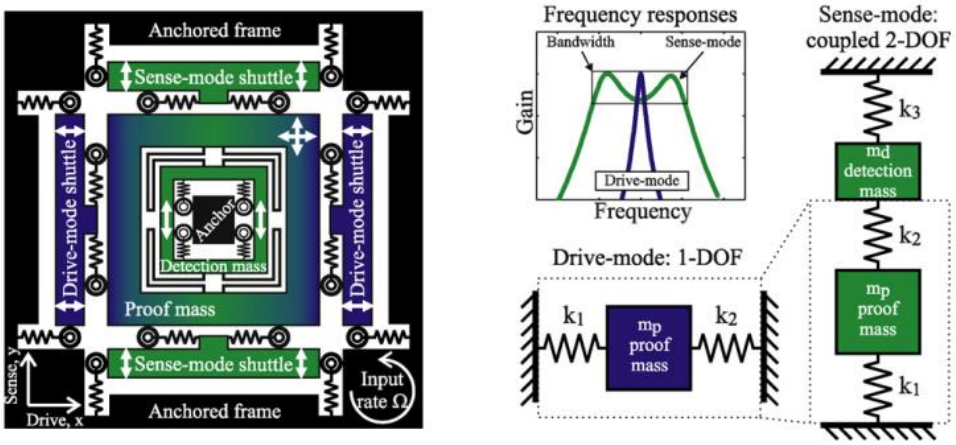

Figure 2.5 Schematics of the proposed MEMS gyroscope and (b) drive-mode model and sense-mode models [61]

From the figure 2.5 the mass m_p forms the drive mode, with single -DoF and having the stiffness values of k_1 and k_2 while the masses m_p and m_d forms the two degree of freedom sense modes having the stiffness values of k_1, k_2 and k_3. The five parameters, m_d, m_p, k_1, $k_2$and k_3 control the position of the resonant frequency for the drive mode which is the operative frequency of the gyroscope. They also control the bandwidth of the gyroscope by changing the position of the sense mode resonant peaks on the frequency spectrum.

[62] figure 2.6 represented the design of the Nickle based gyroscope fabricated using the MetalMUMPs process. The design utilizes the oscillators having 2-DoF drive and 1-DoF sense modes. It uses chevron fashioned thermal actuators to drive the gyroscope in drive direction. The actuators those on work on thermal principle provide the greater force, also these actuators are easy to fabricate with this particular microfabrication process. Another advantage this approach is that the device is also compatible with IC technology. Concept of dynamic amplification is used in the drive mode by utilizing the active -passive mass configuration for improving the device sensitivity.

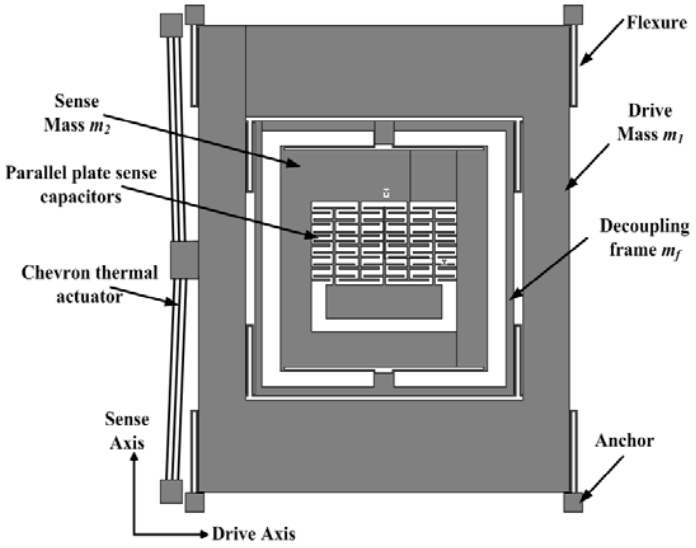

Figure 2.6 Gyroscope model having 2-DoF oscillator in drive and 1-DoF oscillator in sense direction. [62]

To enhance the robustness of the device, the frequency of the sense mode is placed nearly in the central region of operational area, where the amplitude of response is indifferent to structural parameter variations.

The power consumption of the device is estimated as 0.26 watts and the size of the device is 2.6 x 2.2 mm^2 which is about one third of the existing devices. The commercially available microfabrication process of metalMUMPs also provides additional benefit of being a cost-effective process.

[63] represented the electrostatically driven 3-DOF gyroscope (non-resonant), having dynamic amplification in it drive mode having 2-DOF, fabricated using the fabrication process of metalMUMPs which is available commercially having the 20μm structural layer thickness as shown in figure 2.7. The design utilized the standard micromachining process of electroplated nickel. The operational bandwidth of the system was reported to be 1.74 kHz and dynamically improved gain of 0.2μm is attained. No feedback control has been used in the design to enhance the performance of the device.

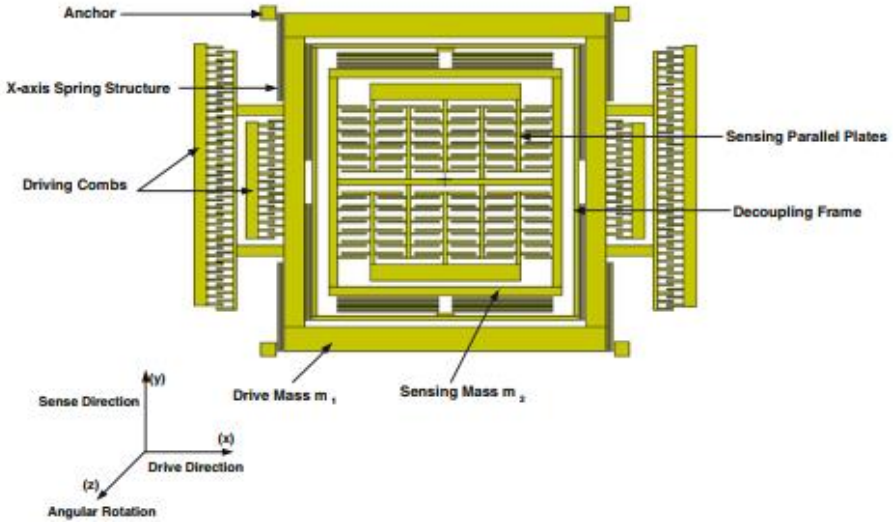

Figure 2.7 Designed model of gyroscope, drive and sense oscillator modes of 2-DoF and 1-DoF respectively [63]

Following the design rules, the complete size of the device was 2.4 x1.6mm. The Monte Carlo analysis and design sensitivity analysis were carried out to show that the gyro is operated with nearly no cross-coupling in the drive mode and in sense mode even in the worst cases, this removes the requirement of the control techniques.

[64] reported the MEMS gyroscope will overall 3-DOF, drive mode with 2-DoF shown in figure 2.8. Device utilized the configuration of active-passive masses to achieved the dynamic amplification. The device was fabricated using the commercially available microfabrication process of MetalMUMPS having the structural thickness of 20 μm and nickel as the structural material for the device.

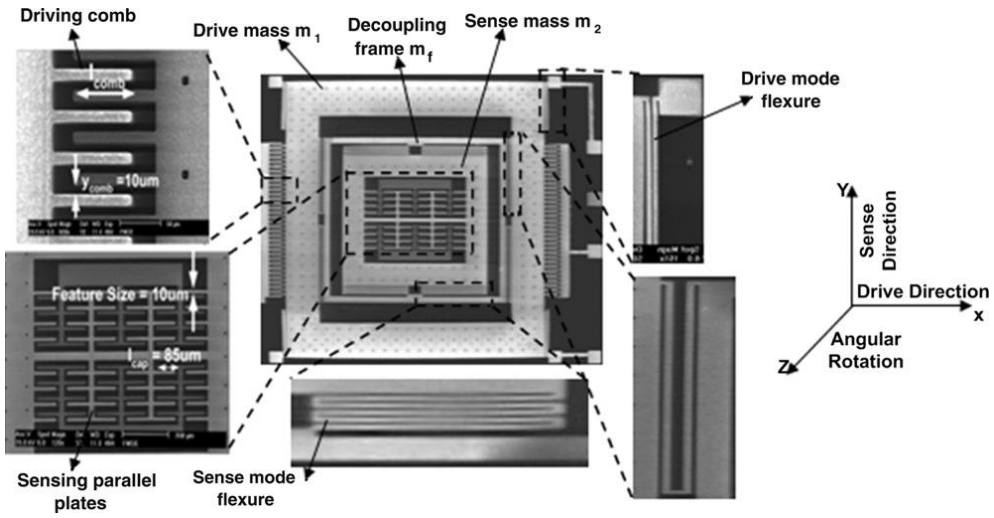

Figure 2.8 MEMS gyroscope with overall 3-DOF, 2-DoF in drive mode [64]

Concept of dynamic amplification has been utilized, large amplitudes of sense mass in drive mode has been achieved with small actuation amplitudes, comb drive electrostatic actuation mechanism has been utilized for actuation purpose. Beams, comb-drive, slide-film model of damping and squeeze-film model of damping are the main components used in modeling.

A detailed damping analysis has been performed and a mathematical model has been proposed to estimate the damping involved in the operation of the gyroscope. Total damping for mass m_1 in drive direction could be approximated as total of the damping due to slide-film between the related mass and its substrate and also between the comb-drive fingers which is represented by coefficient of the damping c_{1x}. Similarly, the slide-film damping for the mass m_2 in drive direction could be estimated as damping between the substrate and the mass and also between the sense capacitor electrodes which is represented as c_{2x}. The damping in the sense mode is due to the mass m_2 and it is the damping due to the slide-film between the substrate and mass in addition to the squeeze-film damping between the sensing parallel plates, this total damping in sense direction is represented by damping coefficient c_{2y}.

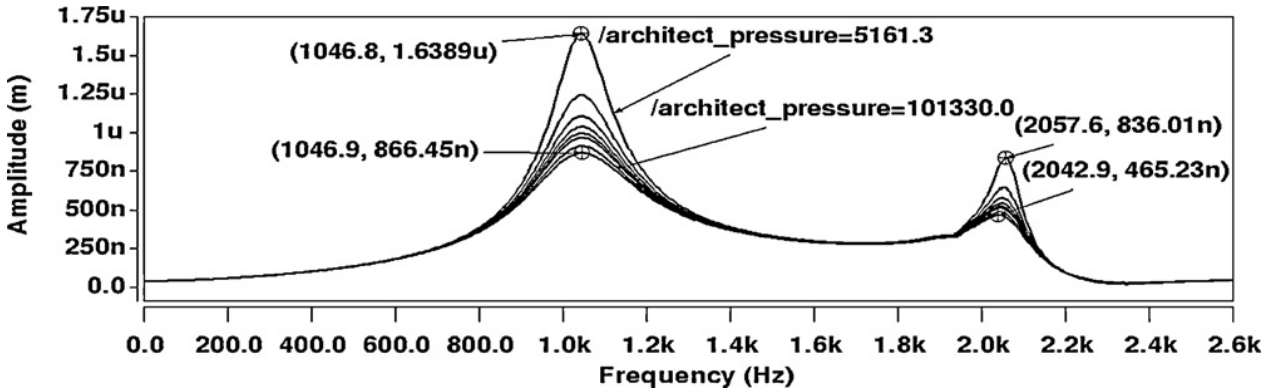

Figure 2.9 Passive mass frequency response in drive mode by varying pressure [64]

Figure [2.9] shows that the gain in the nearly even operational region is indifferent to environmental disturbances like pressure variations and the variations in the damping. Utilizing this approach would be beneficial for the future work.

Chapter 3: Finite Element Method Based Modelling

In this chapter, the proposed architecture of the multi-degree-of-freedom (multi-DoF) MEMS vibratory gyroscope is presented. Detailed mathematical model of the device is discussed. Then, stiffness calculation of the mechanical springs, damping calculation and calculation for the capacitance change is presented. In the end of this chapter the parametric optimization is presented for the structural parameters of the designed gyroscope.

3.1 Structural Design of the Proposed Gyroscope

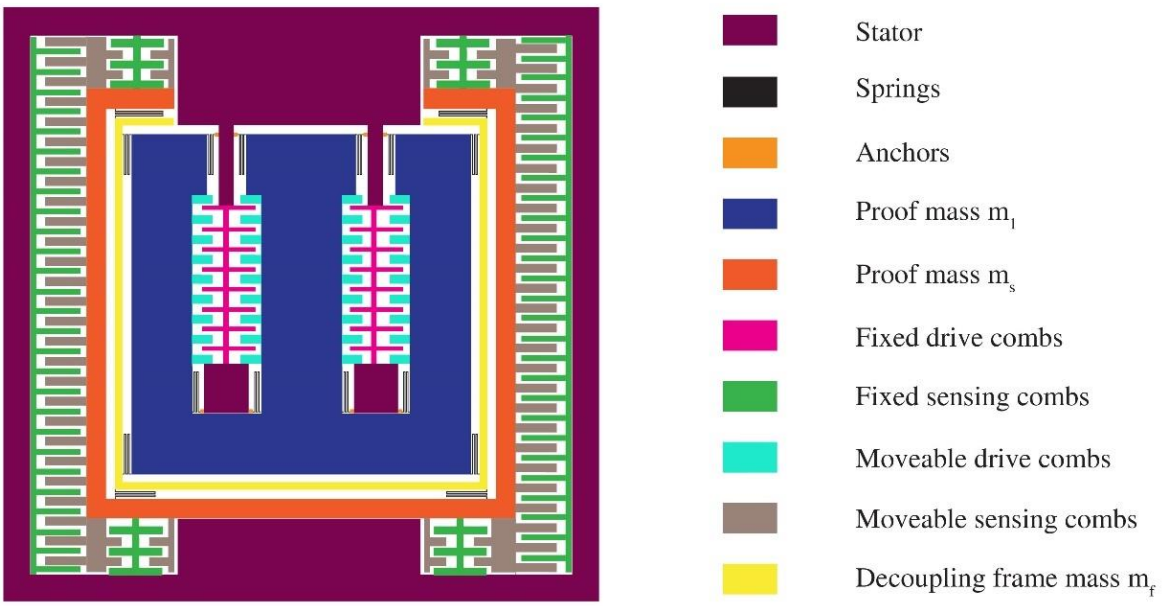

Figure 3.1 Proposed design of the multi-DoF, MEMS gyroscope having single DoF sense mode and 2-DoF drive mode

Figure 3.1 represents the schematic of the anticipated multi-DoF MEMS vibratory gyroscope having the single degree-of-freedom in sense mode and two degree-of-freedom drive mode. Serpentine shaped mechanical spring have been used to attach the drive and the sense masses to each other. These types of spring have been used to minimized the cross-axis displacement in the device. These mechanical-flexures allow the movement of the masses in the chosen direction only. The inner most mass m_1 is known as drive mass and it is attached with the comb drive electrostatic actuators. The mass m_1 oscillate in drive direction (x-axis) by these electrostatic actuator and constraint its movement in the sense direction (y-axis). The outer most mass m_s, sense mass can move in both directions of x-axis and y-axis. The gyroscope works in the configuration of active -passive mass combination. In the 2-DoF system of the gyroscope, the inner most drive mass m_1 forms the active mass and the decoupling frame mass along with the sense mass ($m_2 = m_f + m_s$) form the passive mass of the gyroscope .The passive mass m_2 act as the dynamic vibration absorber (DVA) for the active mass m_1 to achieve the amplified response in the sense direction, Dynamic amplification is achieved in the drive direction with the help of this active -passive mass configuration . Mass m_f is defined as the unidirectional decoupling frame and is used to decouple the drive mass from the sense mass. For improved sensitivity, the concept of the resonance is utilized in the sense mode but this concept is not utilized in the drive mode to maintain the concept of the robust operation in the valley. The outer most mass m_s, known as the sense mass is equipped with the parallel plate sensing combs and they detect the amplitudes of the sense mass corresponding to the input angular velocity. These parallel palate sensing combs have been arranged in the gap-antigap configuration. The minimum allowable air gap as defined by the fabrication process is $2\mu m$.To avoid the Brownian noise, air damping effect and to meet the microfabrication process constraints, the larger gap $d_2$is kept as 9 μm and smaller gap d_1 is kept at 3 μm.

3.2 Analytical Modeling of the Proposed Gyroscope

This section deals with the analytical modeling of the proposed multi-degree of freedom gyroscope.

3.2.1 Equations of Motion for the Different Mode Oscillators

Figure 3.2 shows the mass-spring-damper model (a) drive mode with 2-DoF and (b) sense mode with 1-DoF. In figure 3.2(a), driving force $F_d cos\ (\omega t)$ is applied to the drive mass, the inner most mass of the gyroscope, in the drive direction (x-axis). x_1 is the displacement of the mass m_1 and x_2 is the displacement of the mass m_2. The mechanical springs k_{1x} is used to anchor the driving mass with the substrate. Mechanical springs k_{2x} is used to attach the mass m_1 with the decoupling frame m_f.The mechanical spring k_{2x} allows us to optimize the size of the valley which is the operational region and lies between the resonance-peaks of drive mode oscillating masses. c_{1x} is the air damping of the comb drives attached with the drive mass and c_{2x} is the damping present due to the air and present between the parallel-plates for sensing attached with sense-mass.

In figure 3.2(b), sense mode model is shown. k_y is the mechanical spring which anchor the sense mass m_s with substrate c_y is the damping of air present between the sensing parallel-plates.

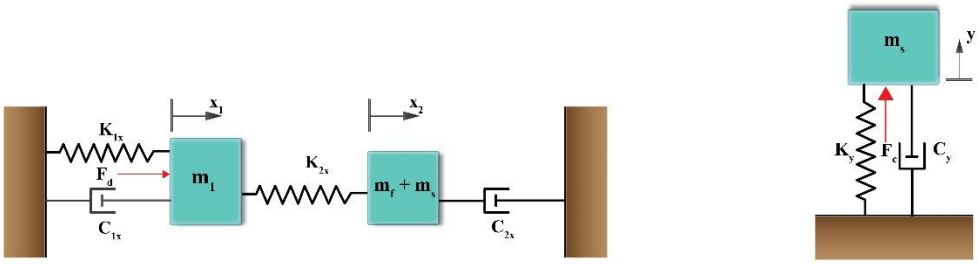

(a) (b)

Figure 3.2 Mass-spring-damper model for projected gyroscope (a) drive mode with 2-DoF, (b) sense mode with 1-DoF

The active-mass m_1, the passive-mass $m_2 = m_f + m_s$ and the sense mass m_s when subjected to the angular velocity Ω_z about the z-axis, the equations-of-motion for these masses are given below.

$$m_1\ddot{x}_1 + c_{1x}\dot{x}_1 + k_{1x}x_1 + k_{2x}\,(x_1 + x_2) = F_D \tag{3.1}$$

$$m_2\ddot{x}_2 + c_{2x}\dot{x}_2 + k_{2x}(x_2 - x_1) = 0 \tag{3.2}$$

$$m_s\ddot{y} + c_y\dot{y} + k_y y = F_c \tag{3.3}$$

Here $F_D = F_d \cos(\omega t)$, the actuation force which acts on the inner mass m_1. $F_c = 2m_s\Omega\dot{x}_2$ is the force acting on the sense mass m_s and is known as the Coriolis force.

3.2.2 Calculation of the Mechanical Stiffness

In the proposed gyroscope the suspension system is intended in a way that the masses m_1 and m_2 formed the 2-DoF drive-mode (x-axis) and 1-DoF sense-mode (y-axis). For the movement in the x-direction there are two sets of the springs that are attached with the masses and for the y-direction movement there is a single set of springs that allow the movement of a sense mass in sense direction. k_{1x} is the set of mechanical-springs, having 4-folds, length of the l_{1x} and width of w, attach the mass m_1 with the substrate. These sets of k_{1x} mechanical-springs allowed the movement of mass m_1 in drive direction only. similarly, the k_{2x} is the set of mechanical-springs having 4-folds, length of l_{2x} and width of w, attach the decoupling frame m_f with the drive mass m_1. Finally, the set of mechanical-springs k_y, having 4-folds, length of l_y and flexure beam width of w, attach the same decoupling frame with the sense mass m_s. The movement of the sense mass in the x-direction is restricted by these set of mechanical-springs, k_y. But the sense mass along with the decoupling-frame moves together in the same direction as drive orientation and act as the single mass as m_2. These k_y mechanical-flexures allow the movement of the sense mass only in the sense orientation (y-axis). All of these beams could be shown as the fixed, guided beams, and their respective stiffness of these beams could be modeled as [68]

$$k_{1x} = \frac{8}{4}\left(\frac{12EI}{L_{1x}^3}\right) \tag{3.4}$$

$$k_{2x} = \frac{4}{4}\left(\frac{12EI}{L_{2x}^3}\right) \tag{3.5}$$

$$k_y = \frac{4}{4}\left(\frac{12EI}{L_y^3}\right) \tag{3.6}$$

Where "E" is the young's modulus of the material, "$I = \frac{w^3 t}{12}$," second moment of inertia of beam cross-section, "w" is the width, "t" is the thickness, " l" is the length of the spring. $\frac{ß}{\gamma}$ is the representation of the values outside the brackets. ß represents the no. of the specific springs and γ represents the no. of folds of each spring.

.

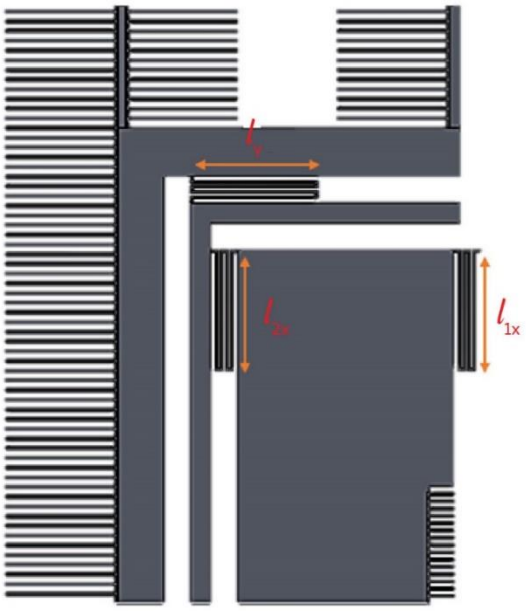

Figure 3.3 The suspension system configuration for the proposed MEMS gyroscope

3.2.3 Calculation for Differential Capacitance Change

Due to the input angular-rotation about the z-axis, a force known as Coriolis force is produced and act on the sense mass m_s in y-direction in case of the proposed gyroscope. Due to the Coriolis force produced, the amplitude "y" is observed in the y-axis, sense direction. The sense mass has the sensing parallel plates attached with it and these are arranged in the differential, gap-antigap configuration. In correspondence to displacement of the sense mass, the total capacitance change could be calculated as [69]

$$\Delta C = \frac{2y \in_0 l_0 t N(d_2^2 - d_1^2)}{(d_2^2 - y^2)(d_1^2 - y^2)} \tag{3.7}$$

where sense direction displacement is represented as y ,$\in_0$ is the permittivity of the free-space, l_0 is the overlapping length of moving plates and fixed parallel plates, t is parallel plates thickness, N is the total no. of plates (parallel), smaller air gap is d_1 and larger air gap between the parallel plates is d_2.

3.2.4 Analysis for Damping

The dissipation of energy in the gyroscope is due to the two types of the damping present, Slide and squeeze film damping of air. Slide-film damping of air contributes in the direction of the drive , both combs for the drive and the parallel-plates for sense moves alongside in x-direction and slides over the plates those are fixed and are parallel to each other. Squeeze-film damping of air contributes in sense direction when moving-parallel-plates moves towards the fixed-parallel-plates and they squeeze the tiny film of air present between these plates. The squeezed-film b_{sq}damping and slide-film b_{sl} damping could be calculated as [70,71].

$$b_{sq} = N_s u_{eff} l_0 t^3 (\frac{1}{d_1^3} + \frac{1}{d_2^3}) \tag{3.8}$$

$$b_{sl} = N u_{eff} A (\frac{1}{d_1} + \frac{1}{d_2}) \tag{3.9}$$

Where $N_s$is the no. of sensing-parallel-plates, u_{eff} is the effective viscosity of air, l_0 is the over-lap length of parallel plates, t is the thickness, A is the over-lap area for the plates (parallel), $d_1$is the smaller gap and $d_2$is the larger air gap. N is the total no. of moving-combs attached with mass. In the drive direction, $d_1 = d_2 = d = 3\mu m$ while in sense direction $d_1 = 3\mu m$ and $d_2 = 9\mu m$.

The relation between the oscillating frequency and the damping-force is represented by the dimensionless squeeze no. σ, that defines the relative effect of air damping force is given as

$$\sigma = \frac{12 u_{eff}\, t^2 \omega}{P d_1^2} \tag{3.10}$$

The characteristic length t represents the thickness of the of plates (parallel-plates) in the proposed gyroscope, ω is the operating frequency of the proposed gyroscope, u_{eff} represents the effective viscosity of air, P represents the pressure of the air and d_1 is the smaller air gap.

3.2.5 Interface Circuitry

For the conversion of the capacitance change in to the equivalent voltage due to the input rotation about the z-axis of the gyroscope, a commercially available IC of MS3110, known as the capacitance to voltage conversion IC is used. This IC supports an no. of MEMS devices those require very high-resolution capacitive readout electronics interface. MEMS sensors need such ICs to sense very small capacitive changes.MS3110 can sense capacitive change of as small as 4 aF/rtHz. Output voltage could be calculated as

$$V_0 = 1.14 \times (G) \times (V2P25) \times \frac{2\Delta C + (CS2 - CS1)}{C_F} + V_{ref} \tag{3.11}$$

where (G) is the gain with a value of 2, $(V2P25)$ is 2.25 and also the value of V_{ref} is 2.25V, ΔC represents the change in capacitance and C_F is the capacitor for the feedback and having the value of 2.8 pF

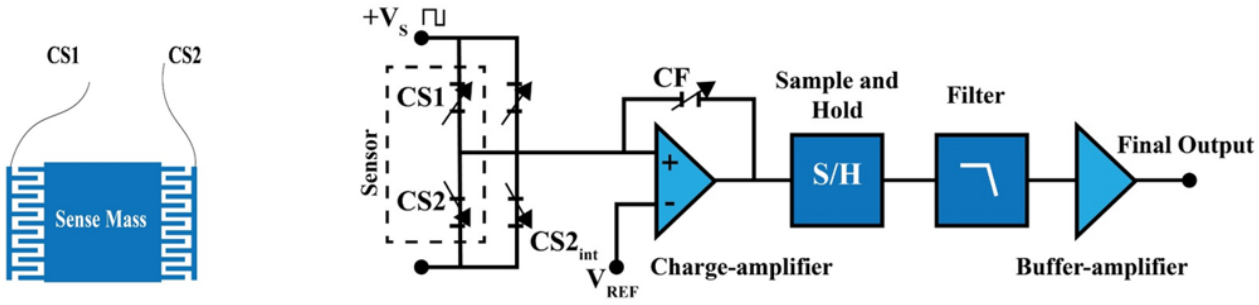

Figure 3.4 MS3110 capacitance to voltage convertor

3.3 Parametric Optimization of the Proposed Gyroscope.

The foremost mechanical factor that is the considered as the measure for the performance-parameter of the designed gyroscope is the movement of the mass (sense-mass) in y-direction. Therefore, there is need to optimized the parameters of the dynamic system to maximized the oscillation amplitudes of the sense mass in y-direction which is the sense-direction.

The larger bandwidth and the enhanced amplitude are the two major requirements of the system. However, the optimal compromise between the both must be obtained to maintain the robust working operation against the parametric fluctuations. The major factors, mass ratio, frequency ratio, stiffness of the k_{1x} and k_{2x}, are the ones which effect the response-amplitude and the band-width of the gyroscope. For optimization, the overall 3-DoF dynamic system is divided into 2-DoF drive mode oscillator and 1-DoF sense modes oscillator. Dynamic amplification is achieved with the help of the mass ratio in drive direction. Mass ratio in drive direction is defined as $\mu_x = \frac{m_2}{m_1}$, where $m_2 = m_f + m_s$. For higher mass ratios, the dynamic amplification will be minimum as the difference between the drive and sense mass is negligible. For the maximum amplification the value of the m_1 should be much higher relative to the mass m_2.

Considering the constraints of the die size and performance parameters, the optimal mass ratio value is 0.5446 shown in figure 3.5 and for this mass ratio the dynamic amplification is shown in the figure 3.6. The average dynamic amplification factor in the operating range is 2.89.

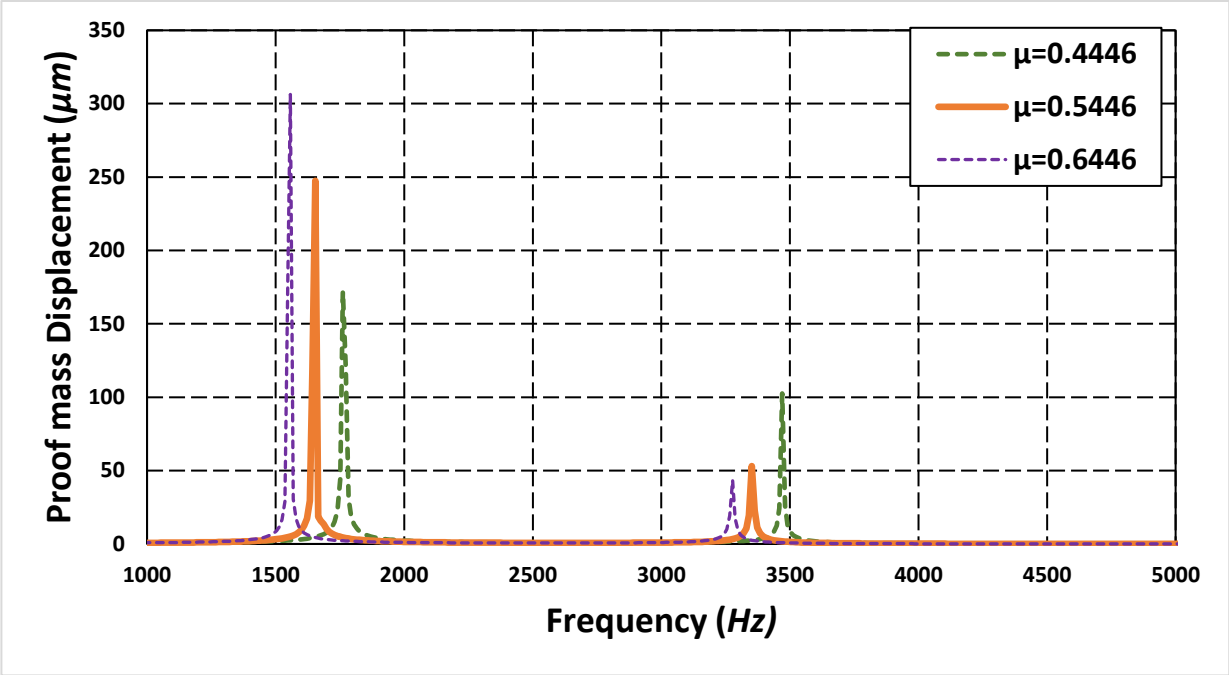

(a)

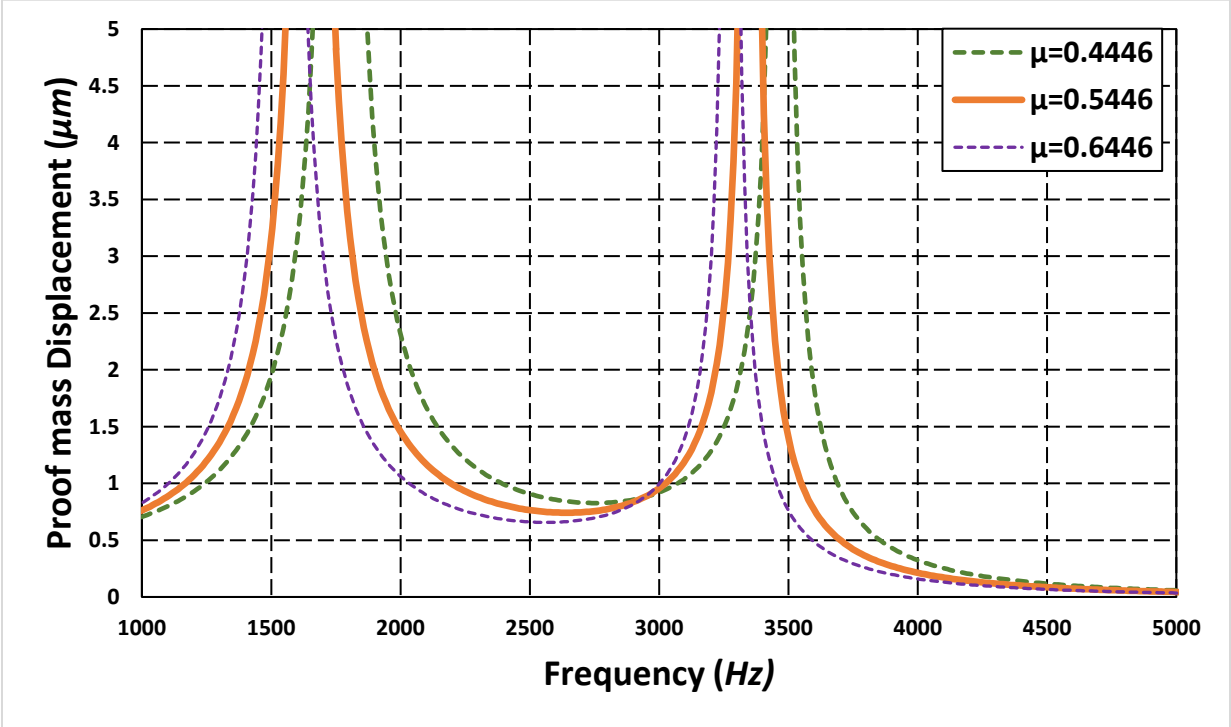

(b)

Figure 3.5 (a) Response of mass ratio on the dynamic amplification of the gyroscope, (b) Response of mass ratio on the dynamic amplification of the gyroscope (zoomed graph)

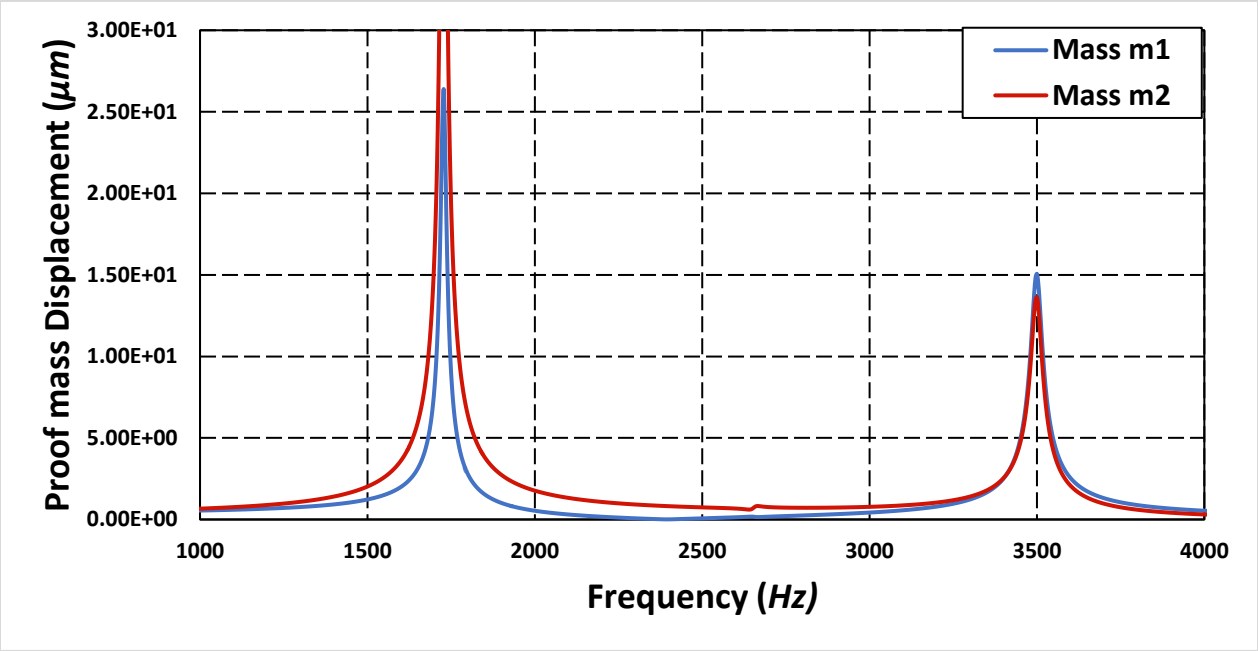

Figure 3.6 Dynamic amplification achieved in drive direction for the proposed gyroscope

To mitigate the parametric variations and the environmental fluctuations, the gyroscopes needs to be operated between the first two resonance peaks of the drive mode. In this flat region between the resonance peaks, these variations and fluctuations have least effect on the performance of the gyroscope. To maximize the gain within the valley (operational-region), parametric optimization is done by varying the values of stiffness for the springs attached to the masses and substrate. Optimized values of the concerned parameters are obtained by varying the one variable at a time and observing its effect on the system, while keeping all other variables constant. The analysis is carried out at the actuation voltages of $10V_{ac}$ and $40V_{dc}$. Figures 3.7 and 3.8 show the operational range and the proposed system response by varying the values of the stiffness of the mechanical springs, k_{1x} and k_{2x}.

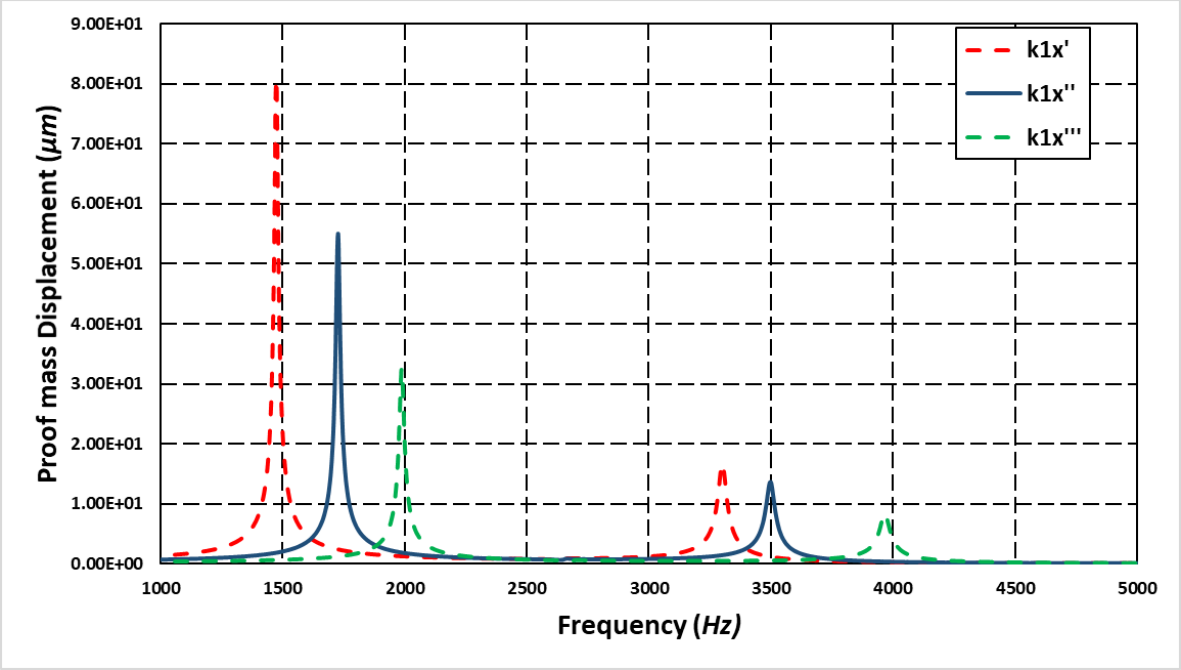

(a)

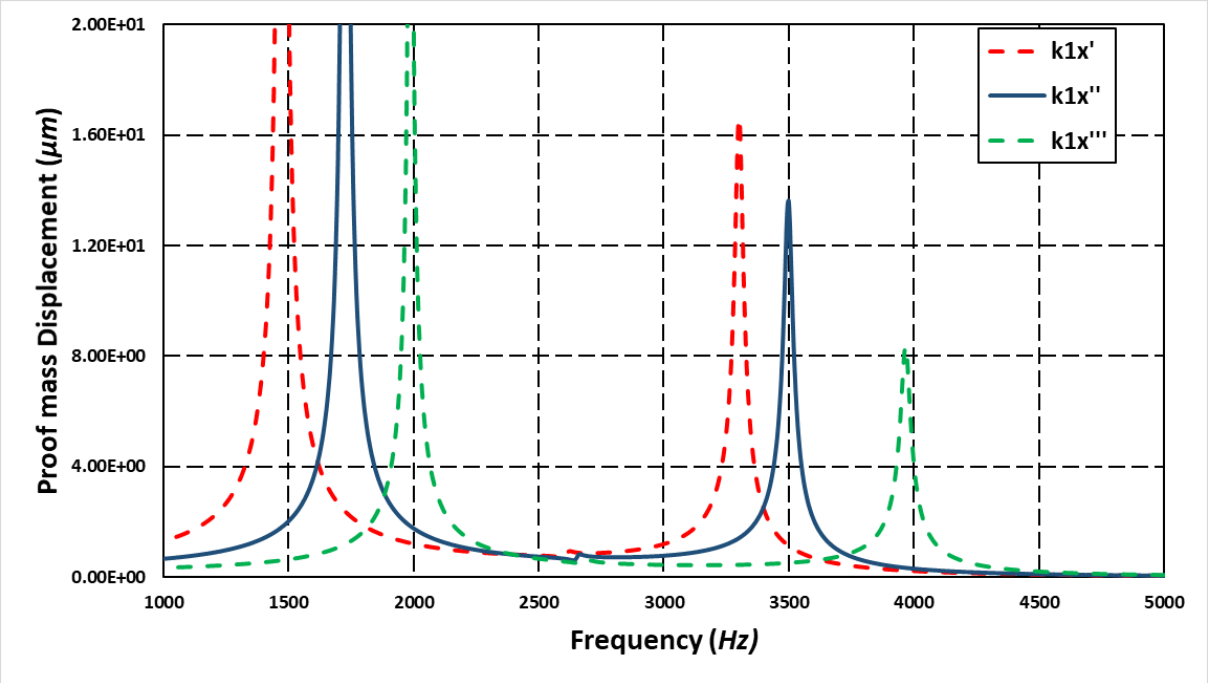

(b)

Figure 3.7 (a) and (b) Graph for optimization of response-amplitude and related bandwidth for varying the value of k_{1x}.

Figure 3.7 (a) and (b) shows the bandwidth and response amplitude graph respectively of the proposed electrostatically driven gyroscope by varying the stiffness of k_{1x}. The graph shows that by increase in the value of the k_{1x}, the values on x-axis of the first peak and second peak of resonance frequencies shifts towards the upper values, that is, the bandwidth shifts as a whole on the frequency spectrum towards right side. While the highest value of the response amplitude has been achieved for a lower value of k_{1x}. By increase in the value of the k_{1x}, shows the decreasing trend of the response amplitudes on the resonance-peaks as shown in figure 3.7(a). By incrementing the k_{1x}, the response-amplitude value with in the operation region between the first and second resonance frequency also decreases as shown in figure 3.7(b).

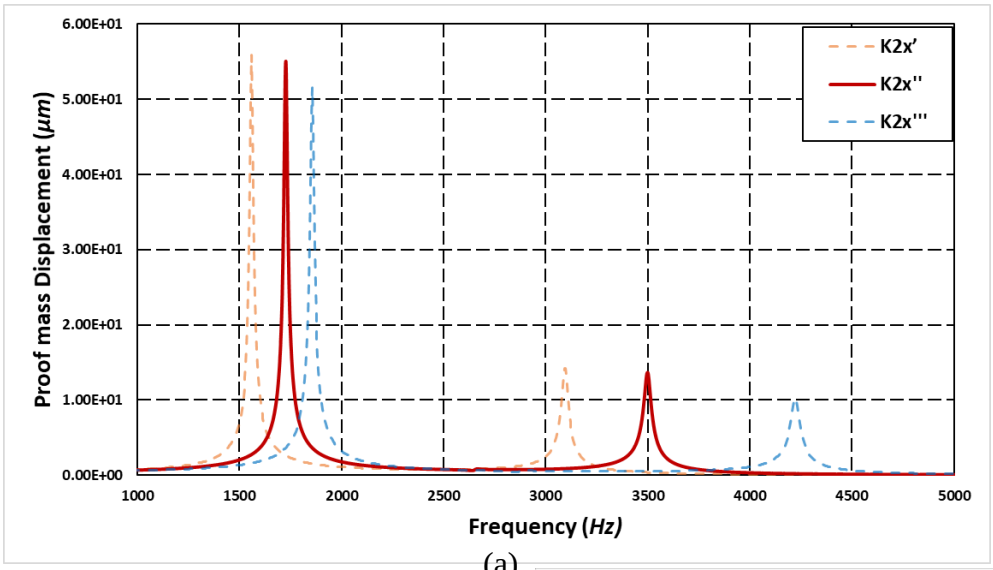

(a)

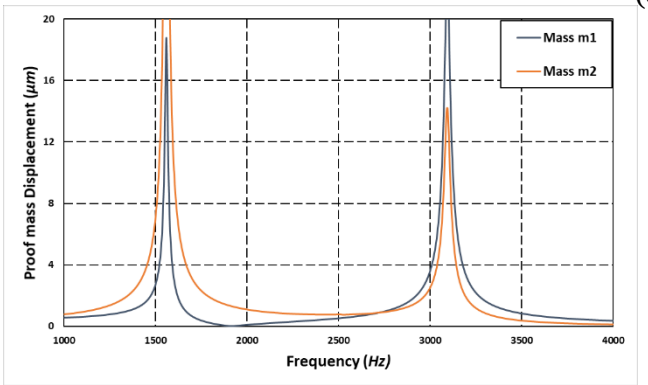

(b)

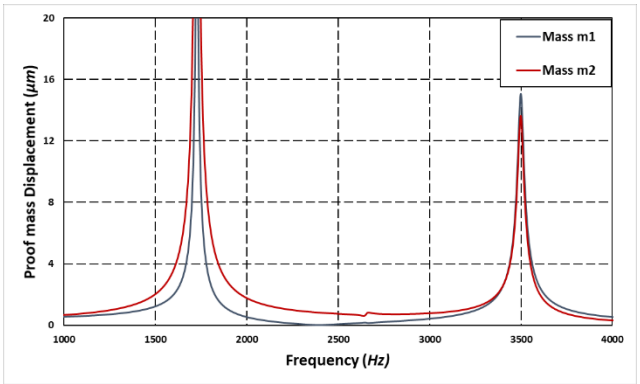

(c)

Figure 3.8 (a), (b) and (c) Graph for optimization of response-amplitude and related bandwidth for varying the value of k_{2x}.

Figure3.8 shows the bandwidth and response amplitude graph of the proposed electrostatically driven gyroscope by varying the stiffness of k_{2x}. (a) shows that the 2nd resonance frequency shifts more left or right side by changing the value of the k_{2x} while little change in the position of the 1st resonance frequency on the frequency spectrum. The value of the k_{2x} greatly affects the bandwidth of the system. By decreasing the value of the k_{2x}, the narrow the band width and also the flat operational region which could be seen in the (b) of figure 3.8. Figure 3.8 (c) shows the optimal value for the bandwidth and the response amplitude in the valley.

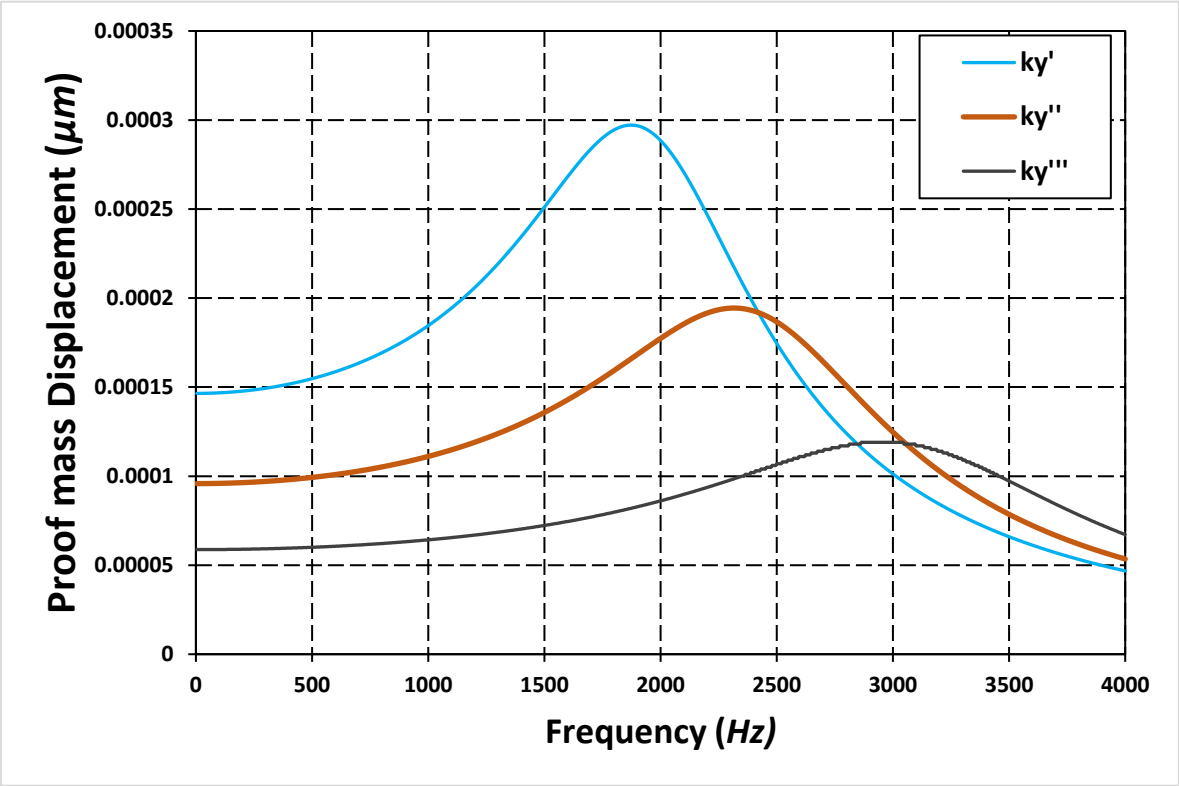

Figure 3.9 Frequency response and the amplitude response of the sense mass in y-direction

Figure3.9: shows the frequency response and amplitude response in the sense direction (y-direction). The Coriolis force induced due to rotation, F_c is the only driving force in the direction of sense mode, and this force is proportional to the oscillation amplitudes of the drive direction.

The main objective or aim of the parametric optimization in the sense direction is to achieve the maximum amplitude keeping the resonant peak with in the operation range of drive mode.

In the case of the proposed MEMS gyroscope, there is single degree-of-freedom (1-DoF) of sense mode and two degree-of-freedom (2-DoF) in drive mode. The operation region is the region from 1st resonance peak to 2nd resonance peak in drive direction. The frequency of the sense mode needed to be within the operational region to avoid any effect due to environmental fluctuations. By increasing the stiffness of the k_y springs, the amplitude reduces and the frequency shifts to the right where there is negligible dynamic amplification is achieved in the drive direction. similarly, if the value of the stiffness for k_y reduces, the amplitude increases reasonably but the frequency shifts to the left and approaches to the region where there are chances that it is affected by the environmental and parametric variations. Therefore, the middle value is selected for maximum gain and to avoid the any effect of environmental fluctuations and parametric variations.

Table 6: Optimized structural parameters for the proposed gyroscope for improved drive mode gain

Parameter	Analytical Value
m_1	2.87×10^{-7}kg
m_2	1.54×10^{-7}kg
m_3	2.92×10^{-8}kg
m_s	1.25×10^{-7}kg
k_{1x}	$67.60\ \mathrm{N}.m^{-1}$
k_{2x}	$33.80\ \mathrm{N}.m^{-1}$
k_y	$29.19\ \mathrm{N}.m^{-1}$
b_{sq}	1.22×10^{-3}
b_{sl}	2.335×10^{-5}

Chapter 4: Finite Element Method Based Modelling

4.1 FEM based Electro-mechanical Analysis

In this chapter, first the modal analysis is performed and the resonant frequencies have been observed and the different modes shapes of the structure. Then the harmonic analysis is performed on the proposed dynamic system of the proposed gyroscope to study the frequency response.
The material properties of the SOIMUMPs silicon for the FEM-based simulations are recorded in Table 7.

Table 7: Material properties of SOIMUMPS

Property	**Value**	**Unit**
Density	2500	$\mathrm{kg.m^3}$
Poisson Ratio	0.29	-
Young's Modulus	169×10^9	$\mathrm{N.m^2}$

4.1.1 Modal Analysis

A finite element based (FEM) modal analysis is performed. This modal analysis is performed to verify and also validate the resonance frequencies obtained by the developed analytical model. The inputs for this analysis are the material properties and the boundary conditions whereas the resonant frequencies and mode shapes are the output-responses for the analysis. Computational time for the analysis is dependent on the meshing size and have a vital role in modal and the harmonic analysis. The chosen meshing size is based upon the patch performing algorithm which is used for controlling the tetrahedrons size. Figure 4.1-4.3 shows the different resonant frequencies and respected allied mode shapes. Table-8 show the comparison of the drive-mode and sense-mode resonance-frequencies peaks obtained by the analytical modal and by FEM-based simulations. The difference between the analytical values and the FEM simulations is less than the 2%, which validates that the developed mathematical model is correct.

.

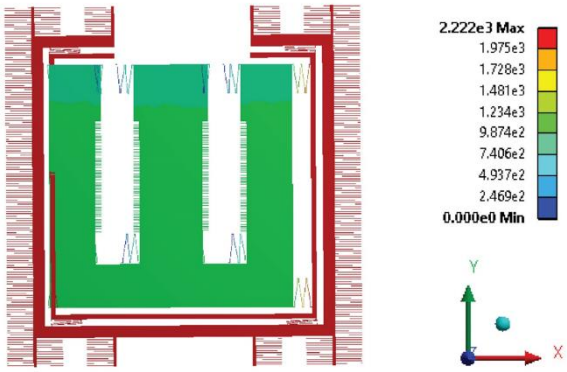

Figure 4.1 1st drive mode at resonance frequency of 1727 Hz

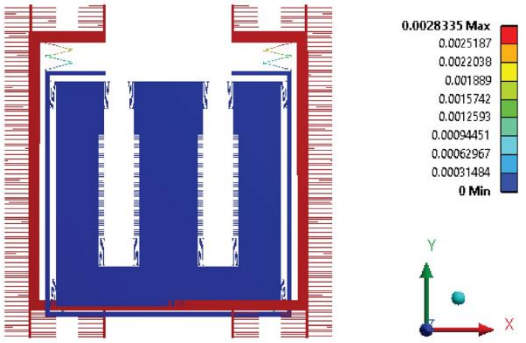

Figure 4.2 Sense mode at resonance frequency of 2369 Hz

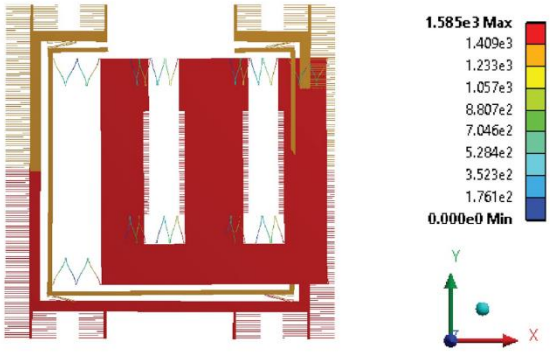

Figure 4.3 2nd drive mode at resonance frequency of 3499 Hz.

Table 8: Comparison of modal analysis results of mathematical model and FEM Simulations

Resonant Frequency	**Finite Element Analysis (FEM) (Hz)**	**Analytical Modal (Hz)**	**Difference in percentage**
1^{st} Drive Mode	1727	1728	0.057 %
Sense Mode	2369	2342	1.15 %
2^{nd} Drive Mode	3499	3496	0.085 %

4.1.2 Harmonic Response Analysis

Harmonic analysis was performed on the proposed gyroscope to analyzed the frequency-response. A $40V_{dc}$ and $10V_{ac}$ actuation voltage is applied to accomplish the harmonic-response analysis. The damping present in the device due to air pressure greatly effects the amplitude-response of the gyroscope.

In the case of the harmonic-analysis, different damping coefficient values used, have been assimilated by the equation represented in section 3.2. Frequency-response for the drive mode of the two proof masses m_1 and m_2, using the FEM based simulations is shown in Figure 4.4.

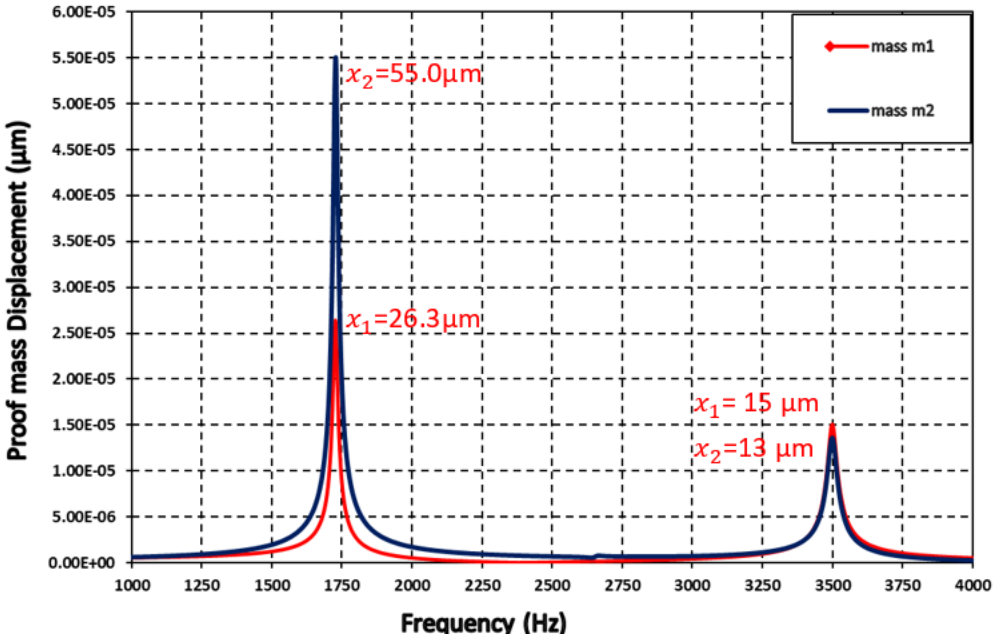

Figure 4.4 Drive mode frequency response

At 1st resonance peak at resonance frequency of 1727 Hz, mass m_2 moves 5.50 x10^{-5} m and mass m_1 moves to 2.63 x 10^{-5} m which gives us the amplification ratio of 2.09, while at 2nd resonance peak at resonance frequency of 3499 Hz, mass m_2 moves 1.36 x 10^{-5}m and mass m_1 moves 1.51 x 10^{-5} m, so there is no dynamic amplification at this point is achieved. Within the valley (flat operation region) the average value for the dynamic amplification ratio is 2.89.

The most appropriate region for the robust-operation of the gyroscope is the flat-region between the 1st and 2nd resonance-frequencies where the environmental changes and the parametric fluctuations have minimum effect on performance of gyroscope. So, the sense mass m_s and related suspension system in the sense direction i-e along y-axis are adjusted for the sense mode peak position that is 2369 Hz, nearly the center of the operational region between the two resonance-peaks of drive modes.

Figure 4.5 shows that the resonance frequency for the sense mode lies at 2396 Hz for ambient settings.

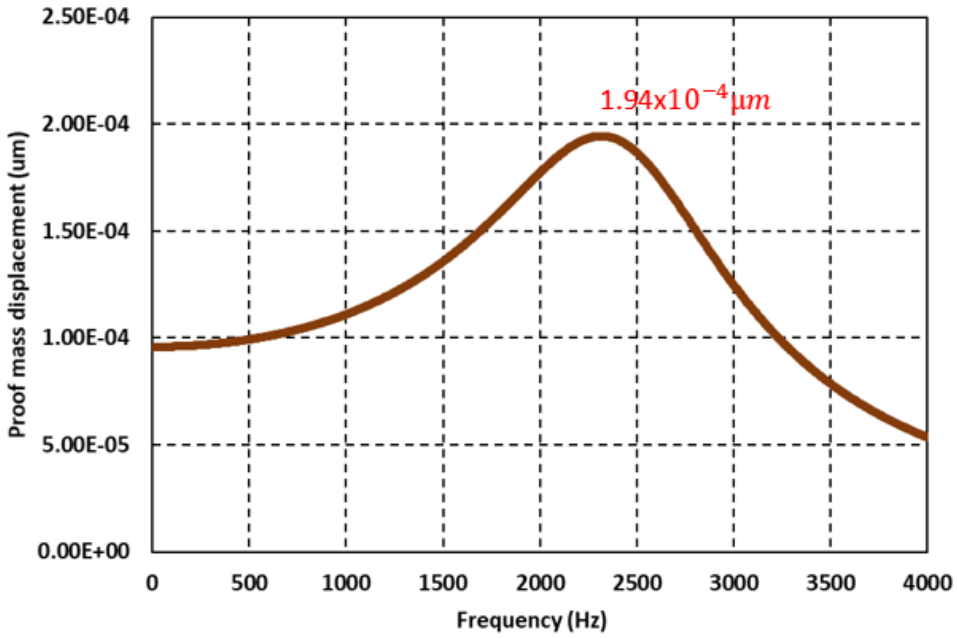

Figure 4.5 Sense mode resonance frequency for ambient settings

Chapter 5: Conclusion

In this research work, a complete architecture of a multi-degree-of-freedom with drive-mode having 2-DoF and a sense-mode with 1-DoF is presented. The gyroscope is designed by carefully considering the design-rules of the commercially offered and a cost-effective multi-user foundry process of SOIMUMPs offered by MEMSCAPS Inc. operational in the United States. The operational bandwidth of the gyroscope is 1772 Hz and the amplification ratio of 2.98 in drive direction.

The reliability of the MEMS gyroscope is key performance parameter and is dependent on the design of the device and also on the material properties used to fabricate that device. Table 9 shows that in the literature, most of the available non-resonant gyroscopes used Nickle or silicon thin films as structure material.

Table 9: Comparison of Proposed Design with Existing Designs

	Structural Layer					
Reference	**Material**	**Thickness (um)**	**Configuration**	**Device Size**	**Sensitivity**	**Bandwidth**
Schofield et al. [11]	*Silicon*	75	$1-DoF\ Drive$ $2-DoF\ Sense$	-	$2.3\ \mu V/(^{\circ}/s)$	$600\ Hz$
Trusov et al. [26]	*Silicon*	50	$1-DoF\ Drive$ $2-DoF\ Sense$	$3\times 3\ mm^2$	$56\ \mu V/(^{\circ}/s)$	$250\ Hz$
Acar et al. [7]	*Ploysilicon*	100	$1-DoF\ Drive$ $2-DoF\ Sense$	$4\times 4\ mm^2$	$0.0303 mV/(^{\circ}/s)$	$50\ Hz$
This work	*Silicon*	25	$1-DoF\ Drive$ $2-DoF\ Sense$	$3.97\times 4.0\ mm^2$	$8.9\times 10^{-16}\ F/(^{\circ}/s)$ $3.27\ mV/(^{\circ}/s)$ $1.94\times 10^{-4}\ \mu m/(^{\circ}/s)$	$1772\ Hz$

Majority of the multi-DoF MEMS gyroscopes presented in literature those use silicon as structural material had been fabricated using the in-house microfabrication process. To develop this in-house microfabrication facility involves very high costs. This could be one of the major reasons that limited research work has been done in development of Non-resonant gyroscopes. Problem to this solution is the multiuser MEMS microfabrication process, which allow to use silicon structural layer having the thickness of 10μm or 25μm. This process is commercially available but with some design rules as discussed in section 1.5. Proposed design of the gyroscope not only follows these design rules but also achieve much better performance. The voltage sensitivity of 3.27 mV/º/s has been achieved and the dynamic range of the proposed gyroscope is estimated as 88.94 dB with minimum angular rate of 0.184 $°/s$ and max angular rate of 5154.6 $°/s$

Completion Certificate

It is certified that the contents of thesis document titled "***Design and Analysis of Multi-DoF MEMS Gyroscope for Inertial Navigation using SOI-MUMPs Fabrication Process***" submitted by NS Adnan Shujah, Registration No. 0000205605 have been found satisfactory in all respects as per the requirements of Main Office, NUST (Exam branch).

Supervisor: _____

Dr. Muhammad Mubasher Saleem

Date: ____ December, 2020

References

[1] Feynman, R. P. (1992). There's plenty of room at the bottom [data storage]. *Journal of microelectromechanical systems*, *1*(1), 60-66.

[2] Madou, M. J. (2002). Fundamentals of Microfabrication: The Science of Miniaturization CRC. *Boca Raton*.

[3] Nguyen, N. T., Shaegh, S. A. M., Kashaninejad, N.and Phan, D. T. (2013). Design, fabrication and characterization of drug delivery systems based on lab-on-a-chip technology. *Advanced drug delivery reviews*, *65*(11-12), 1403-1419.

[4] *Memscap , http://www.memscap.com*

[5] Shkel, A. M., Acar, C.and Painter, C. (2005, October). Two types of micromachined vibratory gyroscopes. In *SENSORS, 2005 IEEE* (pp. 6-pp). IEEE.

[6] Yazdi, N., Ayazi, F.and Najafi, K. (1998). Micromachined inertial sensors. *Proceedings of the IEEE*, *86*(8), 1640-1659.

[7] Acar, C.and Shkel, A. M. (2005). Structurally decoupled micromachined gyroscopes with post-release capacitance enhancement. *Journal of Micromechanics and Microengineering*, *15*(5), 1092.

[8] Azgin, K. I. V. A. N. Ç. (2007). High performance mems gyroscopes. *M. Sc. Thesis*.

[9] Burg, A., Meruani, A., Sandheinrich, B.and Wickmann, M. (2004). MEMS gyroscopes and their applications. *Northwestern University, http://clifton. mech. northwestern. edu/~ me381/project/done/Gyroscope. pdf*.

[10] Shakoor, R. I. (2010). Design, Fabrication And Characterization Of Metalmumps Based Mems Gyroscopes. In *PhD, Chemical and Materials Engineering*. Pakistan Institute Of Engineering And Applied Sciences.

[11] Wu, G. Q., Chua, G. L.and Gu, Y. D. (2017). A dual-mass fully decoupled MEMS gyroscope with wide bandwidth and high linearity. *Sensors and Actuators A: Physical*, *259*, 50-56.

[12] Zhou, J., Jiang, T., Jiao, J. W.and Wu, M. (2014). Design and fabrication of a micromachined gyroscope with high shock resistance. *Microsystem technologies*, *20*(1), 137-144.

[13] Wang, W., Lv, X. and Xu, D. (2014). Design of multi-degree-of-freedom micromachined vibratory gyroscope with double sense-modes. *Measurement*, *58*, 6-11.

[14] Sonmezoglu, S., Alper, S. E. and Akin, T. (2014). An automatically mode-matched MEMS gyroscope with wide and tunable bandwidth. *Journal of microelectromechanical systems*, *23*(2), 284-297.

[15] Zaman, M. F., Sharma, A., Hao, Z. and Ayazi, F. (2008). A mode-matched silicon-yaw tuning-fork gyroscope with subdegree-per-hour Allan deviation bias instability. *Journal of Microelectromechanical systems*, *17*(6), 1526-1536.

[16] Zaman, M. F., Sharma, A. and Ayazi, F. (2006, January). High performance matched-mode tuning fork gyroscope. In *19th IEEE International Conference on Micro Electro Mechanical Systems* (pp. 66-69). IEEE.

[17] Jia, J., Ding, X., Gao, Y. and Li, H. (2018). Automatic Frequency tuning technology for dual-mass MEMS gyroscope based on a quadrature modulation signal. *Micromachines*, *9*(10), 511.

[18] Balachandran, G. K., Petkov, V. P., Mayer, T. and Balslink, T. (2015). A 3-axis gyroscope for electronic stability control with continuous self-test. *IEEE Journal of Solid-State Circuits*, *51*(1), 177-186.

[19] Colinjivadi, K. S., Lee, J. B. and Draper, R. (2008). Viable cell handling with high aspect ratio polymer chopstick gripper mounted on a nano precision manipulator. *Microsystem Technologies*, *14*(9-11), 1627-1633.

[20] Khazaai, J. J., Qu, H., Shillor, M. and Smith, L. (2011, October). Design and fabrication of electro-thermally activated micro gripper with large tip opening and holding force. In *SENSORS, 2011 IEEE* (pp. 1445-1448). IEEE.

[21] Chen, D. S., Yin, C. Y., Lai, R. J. and Tsai, J. C. (2009, January). A multiple degrees of freedom electrothermal actuator for a versatile MEMS gripper. In *2009 IEEE 22nd International Conference on Micro Electro Mechanical Systems* (pp. 1035-1038). IEEE.

[22] Cowen, A., Hames, G., Monk, D., Wilcenski, S. and Hardy, B. (2011). SOIMUMPs design handbook. *MEMSCAP Inc*, 2002-2011.

[23] Zhang, R., Chu, J., Wang, H. and Chen, Z. (2013). A multipurpose electrothermal microgripper for biological micro-manipulation. *Microsystem technologies*, *19*(1), 89-97.

[24] Kim, K., Liu, X., Zhang, Y. and Sun, Y. (2008). Nanonewton force-controlled manipulation of biological cells using a monolithic MEMS microgripper with two-axis force feedback. *Journal of micromechanics and microengineering*, *18*(5), 055013.

[25] Beyeler, F., Neild, A., Oberti, S., Bell, D. J., Sun, Y., Dual, J. and Nelson, B. J. (2007). Monolithically fabricated microgripper with integrated force sensor for manipulating microobjects and biological cells aligned in an ultrasonic field. *Journal of microelectromechanical systems*, *16*(1), 7-15.

[26] Volland, B. E., Heerlein, H. and Rangelow, I. W. (2002). Electrostatically driven microgripper. *Microelectronic engineering*, *61*, 1015-1023.

[27] Roch, I., Bidaud, P., Collard, D. and Buchaillot, L. (2003). Fabrication and characterization of an SU-8 gripper actuated by a shape memory alloy thin film. *Journal of Micromechanics and Microengineering*, *13*(2), 330.

[28] Yang, S. and Xu, Q. (2017). A review on actuation and sensing techniques for MEMS-based microgrippers. *Journal of Micro-Bio Robotics*, *13*(1-4), 1-14.

[29] Solano, B. and Wood, D. (2007). Design and testing of a polymeric microgripper for cell manipulation. *Microelectronic Engineering*, *84*(5-8), 1219-1222.

[30] Khazaai, J. J., Qu, H., Shillor, M. Smith, L. (2011, October). Design and fabrication of electro-thermally activated micro gripper with large tip opening and holding force. In *SENSORS, 2011 IEEE* (pp. 1445-1448). IEEE.

[31] Chang, H., Zhao, H., Ye, F., Yuan, G., Xie, J., Kraft, M. and Yuan, W. (2014). A rotary comb-actuated microgripper with a large displacement range. *Microsystem technologies*, *20*(1), 119-126.

[32] Boudaoud, M., Haddab, Y. and Le Gorrec, Y. (2010, October). Modelling of a MEMS-based microgripper: application to dexterous micromanipulation. In *2010 IEEE/RSJ International Conference on Intelligent Robots and Systems* (pp. 5634-5639). IEEE.

[33] Munasinghe, K. C., Bowatta, B. G. C. T., Abayarathne, H. Y. R., Kumararathna, N., Maduwantha, L. K. A. H., Arachchige, N. M. P. and Amarasinghe, Y. W. R. (2016, April). New MEMS based micro gripper using SMA for micro level object manipulation and assembling. In *2016 Moratuwa Engineering Research Conference (MERCon)* (pp. 36-41). IEEE.

[34] AbuZaiter, A., Nafea, M.and Ali, M. S. M. (2016). Development of a shape-memory-alloy micromanipulator based on integrated bimorph microactuators. *Mechatronics*, *38*, 16-28.

[35] Park, J. and Moon, W. (2003). A hybrid-type micro-gripper with an integrated force sensor. *Microsystem technologies*, *9*(8), 511-519.

[36] Jeon, C. S., Park, J. S., Lee, S. Y. and Moon, C. W. (2007). Fabrication and characteristics of out-of-plane piezoelectric micro grippers using MEMS processes. *Thin Solid Films*, *515*(12), 4901-4904.

[37] Kim, W. H., Park, J. S., Shin, K. S., Park, K. B., Seong, W. K. and Moon, C. W. (2005). Simulation and fabrication of silicon micro-grippers actuated by piezoelectric actuator. In *Materials Science Forum* (Vol. 475, pp. 1885-1888). Trans Tech Publications Ltd.

[38] Kim, D. H., Lee, M. G., Kim, B. and Sun, Y. (2005). A superelastic alloy microgripper with embedded electromagnetic actuators and piezoelectric force sensors: a numerical and experimental study. *Smart materials and structures*, *14*(6), 1265.

[39] Chen, D. S., Yeh, P. F., Chen, Y. F., Tsai, C. W., Yin, C. Y., Lai, R. J. and Tsai, J. C. (2013). An electrothermal actuator with two degrees of freedom serving as the arm of a MEMS gripper. *IEEE Transactions on Industrial Electronics*, *61*(10), 5465-5471.

[40] Sergio, M., Manaresi, N., Tartagni, M., Guerrieri, R. and Canegallo, R. (2002, June). A textile based capacitive pressure sensor. In *SENSORS, 2002 IEEE* (Vol. 2, pp. 1625-1630). IEEE.

[41] Ko, C. T., Tseng, S. H. and Lu, M. S. C. (2006). A CMOS micromachined capacitive tactile sensor with high-frequency output. *Journal of Microelectromechanical Systems*, *15*(6), 1708-1714.

[42] Dürig, U. (2005). Fundamentals of micromechanical thermoelectric sensors. *Journal of Applied Physics*, *98*(4), 044906.

[43] Zhu, Y., Bazaei, A., Moheimani, S. O. R. and Yuce, M. R. (2010). A micromachined nanopositioner with on-chip electrothermal actuation and sensing. *IEEE Electron device letters*, *31*(10), 1161-1163.

[44] Piriyanont, B., Fowler, A. G. and Moheimani, S. R. (2015). Force-controlled MEMS rotary microgripper. *Journal of Microelectromechanical Systems*, *24*(4), 1164-1172.

[45] Mei, T., Ge, Y., Chen, Y., Ni, L., Liao, W. H., Xu, Y. and Li, W. J. (1999, January). Design and fabrication of an integrated three-dimensional tactile sensor for space robotic applications. In *Technical Digest. IEEE International MEMS 99 Conference. Twelfth IEEE International Conference on Micro Electro Mechanical Systems (Cat. No. 99CH36291)* (pp. 112-117). IEEE.

[46] Hasegawa, Y., Shikida, M., Shimizu, T., Miyaji, T., Sasaki, H., Sato, K. and Itoigawa, K. (2004). Amicromachined active tactile sensor for hardness detection. *Sensors and Actuators A: physical*, *114*(2-3), 141-146.

[47] Xu, Q. (2015). Design, fabrication, and testing of an MEMS microgripper with dual-axis force sensor. *IEEE Sensors Journal*, *15*(10), 6017-6026.

[48] Han, K., Lee, S. H., Moon, W. and Park, J. S. (2006, October). Fabrication of the micro-gripper with a force sensor for manipulating a cell. In *2006 SICE-ICASE International Joint Conference* (pp. 5833-5836). IEEE.

[49] Chen, T., Chen, L., Sun, L., Wang, J. and Li, X. (2008, October). A sidewall piezoresistive force sensor used in a MEMS gripper. In *International Conference on Intelligent Robotics and Applications* (pp. 207-216). Springer, Berlin, Heidelberg.

[50] Sonmezoglu, S., Alper, S. E. and Akin, T. (2013, June). A high performance automatic mode-matched MEMS gyroscope with an improved thermal stability of the scale factor. In *2013 Transducers & Eurosensors XXVII: The 17th International Conference on Solid-State Sensors, Actuators and Microsystems (TRANSDUCERS & EUROSENSORS XXVII)* (pp. 2519-2522). IEEE.

[51] Trusov, A. A., Schofield, A. R. and Shkel, A. M. (2011). Micromachined rate gyroscope architecture with ultra-high quality factor and improved mode ordering. *Sensors and Actuators A: Physical*, *165*(1), 26-34.

[52] Shakoor, R. I., Bazaz, S. A., Burnie, M., Lai, Y. and Hasan, M. M. (2011). Electrothermally actuated resonant rate gyroscope fabricated using the MetalMUMPs. *Microelectronics journal*, *42*(4), 585-593.

[53] Nguyen, M. N., Ha, N. S., Nguyen, L. Q., Chu, H. M. and Vu, H. N. (2017). Z-axis micromachined tuning fork gyroscope with low air damping. *Micromachines*, *8*(2), 42.

[54] Li, W., Xiao, D., Wu, X., Su, J., Chen, Z., Hou, Z. and Wang, X. (2017). Enhanced temperature stability of sensitivity for MEMS gyroscope based on frequency mismatch control. *Microsystem Technologies*, *23*(8), 3311-3317.

[55] Park, S. and Horowitz, R. (2003). Adaptive control for the conventional mode of operation of MEMS gyroscopes. *Journal of Microelectromechanical Systems*, *12*(1), 101-108.

[56] Gallacher, B. J., Burdess, J. S. and Harish, K. M. (2006). A control scheme for a MEMS electrostatic resonant gyroscope excited using combined parametric excitation and harmonic forcing. *Journal of Micromechanics and Microengineering*, *16*(2), 320.

[57] Xia, D., Chen, S., Wang, S. and Li, H. (2009). Microgyroscope temperature effects and compensation-control methods. *Sensors*, *9*(10), 8349-8376.

[58] Schofield, A. R., Trusov, A. A. and Shkel, A. M. (2008). Effects of operational frequency scaling in multi-degree of freedom MEMS gyroscopes. *IEEE Sensors Journal*, *8*(10), 1672-1680.

[59] Acar, C. and Shkel, A. M. (2003). Nonresonant micromachined gyroscopes with structural mode-decoupling. *IEEE Sensors Journal*, *3*(4), 497-506.

[60] Acar, C. and Shkel, A. M. (2006). Inherently robust micromachined gyroscopes with 2-DOF sense-mode oscillator. *Journal of Microelectromechanical Systems*, *15*(2), 380-387.

[61] Trusov, A. A., Schofield, A. R. and Shkel, A. M. (2009). Performance characterization of a new temperature-robust gain-bandwidth improved MEMS gyroscope operated in air. *Sensors and Actuators A: Physical*, *155*(1), 16-22.

[62] Shakoor, R. I., Bazaz, S. A., Kraft, M., Lai, Y. and Ul Hassan, M. M. (2009). Thermal actuation based 3-DoF non-resonant microgyroscope using MetalMUMPs. *Sensors*, *9*(4), 2389-2414.

[63] Saleem, M. M. andBazaz, S. A. (2011). Design and robustness analysis of structurally decoupled 3-DoF MEMS gyroscope in the presence of worst-case process tolerances. *Microsystem technologies*, *17*(8), 1381-1391.

[64] Riaz, K., Bazaz, S. A., Saleem, M. M. and Shakoor, R. I. (2011). Design, damping estimation and experimental characterization of decoupled 3-DoF robust MEMS gyroscope. *Sensors and Actuators A: Physical*, *172*(2), 523-532.

[65] Verma, P., Khan, K. Z., Khonina, S. N., Kazanskiy, N. L. and Gopal, R. (2016). Ultraviolet-LIGA-based fabrication and characterization of a nonresonant drive-mode vibratory gyro/accelerometer. *Journal of Micro/Nanolithography, MEMS, and MOEMS*, *15*(3), 035001.

[66] Saqib, M., Mubasher Saleem, M., Mazhar, N., Awan, S. U. andShahbaz Khan, U. (2018). Design and analysis of a high-gain and robust multi-DOF electro-thermally actuated MEMS gyroscope. *Micromachines*, *9*(11), 577.

[67] Dyck, C. W., Allen, J. J. and Huber, R. J. (1999, August). Parallel-plate electrostatic dual-mass resonator. In *Micromachined Devices and Components V* (Vol. 3876, pp. 198-209). International Society for Optics and Photonics.

[68] Young, W. C., Budynas, R. G. and Sadegh, A. M. (2002). *Roark's formulas for stress and strain* (Vol. 7). New York: McGraw-Hill.

[69] Edalatfar, F., Yaghootkar, B., Qureshi, A. Q. A., Azimi, S. and Bahreyni, B. (2016, October). Design, fabrication and characterization of a high performance MEMS accelerometer. In *2016 IEEE SENSORS* (pp. 1-3). IEEE.

[70] Bao, M. and Yang, H. (2007). Squeeze film air damping in MEMS. *Sensors and Actuators A: Physical*, *136*(1), 3-27.

[71] Abdolvand, R., Amini, B. V. and Ayazi, F. (2007). Sub-micro-gravity in-plane accelerometers with reduced capacitive gaps and extra seismic mass. *Journal of microelectromechanical systems*, *16*(5), 1036-1043.